PCCP

Accepted Manuscript

ROYAL SOCIETY OF CHEMISTRY

www.rsc.org/pccp

Cite this: DOI: 10.1039/c0xx00000x

www.rsc.org/xxxxxx

REVIEW

A review on 1-D and 2-D nanostructured materials for hydrogen generation

Veluru Jagadeesh babu[a]*†, Sesha Vempati[a]*†, Tamer Uyar[a,b]*, Seeram Ramakrishna[c]*

Received (in XXX, XXX) Xth XXXXXXXXX 20XX, Accepted Xth XXXXXXXXX 20XX

DOI: 10.1039/b000000x

Hydrogen is considered as an attractive alternative to the present and future fuel/energy demands to substitute fossil fuels because of the environmental considerations in additions to various other advantages. Among a list of H_2 production methods, photocatalysis is one of the economic ways which requires further development so that it can be applied in the industry. In the recent years, one and two dimensional nanostructures in pristine and in modified forms have depicted a great potential in H_2 generation as catalysts. By given the vast amount of literature we aim to review the recent developments of such nanostructure catalysts and their efficacy for H_2 generation under UV/visible/simulated solar light. Despite of the wide research efforts many of the photocatalysts cannot meet the practical requirements such as visible light activity. Note that the H_2 production is dependent on various parameters and factors. In order to meet the energy demands several challenges associated with the H_2 production need to be solved. In this review we have addressed various factors those influence the efficiency of H_2 production and suggested alternatives where possible. The nanostructures are classified based on their morphology and the efficiency is juxtaposed with the influencing parameters. This review further suggests effective ways on engineering a catalyst-combination to overcome the associated performance barriers.

1. Introduction

Hydrogen (H_2) is considered as an ideal fuel for the future energy demands due to its compatibility with environment when sourced from clean and renewable energy resources [1]. H_2 attracted the researchers because of its fascinating features such as unlimited generation from abundant water sources on the earth. Significantly, upon combustion it generates water as an exhaust in contrast to conventional fossil fuels. Furthermore, its gravimetric energy content (heat of combustion) is ~5 times higher than that of methanol and ethanol while ~2.5 times that of hydrocarbons [2]. On the other hand, the lack of natural availability is the greatest disadvantage of this fuel. However, note that it can be produced from renewable and conventional energy sources (solar, wind, hydro power and geothermal, fossil fuels, nuclear, biomass [3]) as presented in Fig.1. Despite the current renewable energy contributes nearly 5% of the overall hydrogen production through water electrolysis while the remaining is mainly derived from fossil fuels [4]. Producing H_2 from fossil fuels may not be economically a wise option because it requires high temperature input for synthesis and emits CO_2 (Ref. [3]). Furthermore, the fossil fuels cannot be replenished easily. Thus H_2 generation from fossil fuels cannot be considered as an environmentally viable option [5]. Among the renewable power sources photocatalytic water splitting offers a promising way for the clean, low-cost and environmentally friendly production of H_2 by solar energy. The nanostructured catalysts possess additional advantages in the photocatalysis [6-11]. At this juncture, photocatalytic H_2 production from water via solar energy is the best alternative. Of course it is one of the attractive and competitive technologies. As the technology advances its implementation and associated costs can be significantly reduced. In 1972 a work by Fujishima and Honda [12] demonstrated photoelectrochemical (PEC) method to split water into H_2 and O_2, where a bias is applied across TiO_2 thin film and Pt counter electrode. Later in 1979, Bard has shown that water can be split into H_2 and O_2 by simply using a powdered TiO_2 and exposing it to the sun light without any bias [13-15] however in the presence of sacrificial reagent (SR).

It is now understood that catalysis takes place on the surface of a semiconductor. When a photon of energy matches or exceeds the band gap energy (E_g) of a semiconductor, an electron is promoted to the conduction band (CB) leaving a hole in the valance band (VB). Essentially, the excited state CB electron and VB hole can recombine or get trapped in a metastable surface state. On the other hand, they can participate in reactions with electron donors and acceptors those adsorbed on the surface of the semiconductor. Under suitable conditions (which will be addressed shortly) the CB electron reduces the H^+ ions to yield H_2 gas and VB hole generates O_2 in a simplistic scenario. Notably the back reactions are possible to form H_2O instead of H_2 gas. It is now convincing that efficient *e/h* pair separation is the crucial

factor for the catalysis. Furthermore, selecting a semiconductor requires prior knowledge about the CB and VB levels with respect to redox potential of H_2O. i.e. CB should be lower than the H^+/H_2 potential and VB should be higher than the OH^-/O_2 potential. The next immediate consideration would be the E_g of the semiconductor which determines the range of wavelength that it can absorb to create *e/h* pairs. Low E_g materials such as ferrous oxide (1.9–2.1 eV), [19] tungsten nitride (2.2 eV) [20] as well as other III–V and II–VI compound semiconductors [21-23] can be active materials within the lines of energetic locations of CB and VB with respect to H_2O redox potential. For some of the semiconductors although their E_g covers the visible part of the solar spectrum, their CB and/or VB levels are not compatible with respect to the redox potential of H_2O. These materials can be photocorrosive; for example MoS_2, Fe_2O_3 and WO_3 where their CB minima is lower than the thermodynamic requirement [24]. It is also notable that such photocorrosive catalysts have been explored after certain modifications such as incorporation of co-catalysts (NiOx, RuO_2 [25, 26] or Rh-Cr), doping with metal ion or combining with other semiconductors [5, 27-29]. The same principle of thermodynamic requirement applies to PEC method as well. [29, 30]. On the other hand t considerable use of small E_g semiconducting materials may cause serious life cycle environmental impacts due to their instability in which casewide E_g materials can be used in H_2 production. Although suitable band positions and stability in the electrolyte favours the large E_g materials (TiO_2, ZnO etc) [30-32]for their absorbance is limited to UV region of the solar spectrum. Despite, a significant solar-to-hydrogen conversion efficiency (η %) of 16.25% is yielded from TiO_2 nanotubes (45 μm) under 100 mW/cm^2 irradiation of UV light (320-400 nm) [33]. Notably here a small fraction (~5%) of available energy in the solar spectrum is utilized. Hence as a solution, wide E_g materials can be subjected to modifications such as doping [34], interfacing with other materials [35, 36] in the form of heterojunction etc. enable the absorption in the visible region or efficiently isolate the *e/h* pairs. This offers clean, cost effective and environmentally benign production of H_2. Izumi et.al[34] studied the visible light response over TiO_2 NTs by anionic (S, N) doping as the most effective method. In ref. [35] it is demonstrated that the heterostructure can cover ~22% of the entire solar spectrum. Sathre et.al[37] analysed the PEC hydrogen production based on fundamental principles. Hisatomi et.al[38] addressed the fundamental aspects of PEC water splitting. The Z-scheme and tandem systems based on multi-step photoexcitation liberate the semiconducting materials from thermodynamic limitations and enable the application of a variety of materials to unassisted water splitting[38].

Semiconducting nanostructures especially in 1D and 2D have shown their superior photocatalytic activity due to improved *e/h* separation and low recombination rate. Ford et.al[16] reported that the by decreasing the diameters of InAs nanowires (NW) the mobility of the electrons can be controlled. While, Martinson et.al[17] compared the transport and recombination dynamics for sintered nanocrystalline particles *versus* nanorod (NR) arrays. In addition core-shell type nanostructures[18] demonstrated enhanced PEC water splitting under solar light. Various architectures of 2D nanosheets with thickness below 100 nm hold great promise for efficient PEC water splitting via . The 2D nanosheets also offer great opportunities such as optimized charge migration, surface modification and light absorption. Zhou et.al [39] addressed the performance of advanced PEC devices related to 2D nanosheets as photoelectrode. Chemically modified nanostructures offer a green and low cost method to generate H_2 fuel *via* PEC water splitting, see a review article by Wang et.al[40]. Liu et.al[41] demonstrated that the Pt-loaded titania hierarchical photonic crystals could double the H_2 evolution in photocatalytic water splitting. The enhancement in H_2 evolution was due to the hierarchical structure that can bring multiple scattering among the photonic crystals and improves the absorbance of light. This provides a strong light harvesting method.

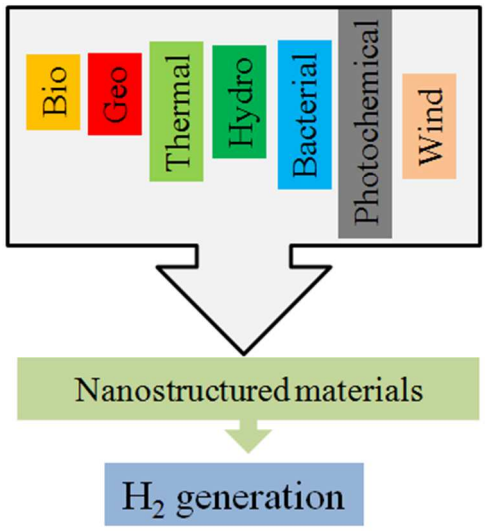

Figure 1: Schematic diagram depicting the various resources for the production of H_2.

In the recent years, the focus of the research is intensified towards nanostructures and their potential applications in future energy needs. Majorly, high specific area provides high density of active sites when compared to their bulk counterparts [42, 43]. The effect of quantum confinement yields significant optical and electronic properties. In the following section, we have elaborated the properties of various types of 1D and 2D semiconducting nanostructures such as NR, NW, nanotubes (NTs), nanofibers (NFs) [44, 45] etc. in the background of H_2 generation.

1.1. Why nanostructures for H_2 generation?

The growing interest in nanostructured metal oxides [46-55] is due to their large surface area (SA), short lateral diffusion length and low reflectivity. Nonetheless most of the metal oxides have large band gap energies leading to the limited light absorption in the visible region. This imposes a fundamental limitation on overall photo-to-hydorgen conversion efficiency. To emphasize, by delaying the recombination of photogenerated *e/h* pair creates the necessary environment so that the exciton pair diffuses to the surface and participate in the catalysis. 1D nanostructures can trap photons more effectively under an appropriate geometric configuration where the carrier diffusion lengths are comparable to their physical dimensions[46]. As a result the photocatalytic

performance is proven to increase significantly [47-55] under reduced dimensions. Therefore, the preparation of nanostructured photocatalysts is indispensable for the future energy demands. This nano dimensions facilitates the efficient collection of free carriers and increases the η [56-58]. Interestingly, the concept of charge carrier generation and subsequent migration is very similar to that of solar cells, where the intrinsic electric field assists the separation. This concept of employing intrinsic electric field is well applied in H_2 generation[59]. Contextually *nn*-type heterojunctions yielded similar results[35]. In the case of photocatalytic H_2 generation, the migration should take place by itself while some assistance may be obtained from the depletion layer (if exists) on the surface. Arrays of NRs have sought considerable interest in the recent past in the context of enhanced absorption of incident light and crystallinity. For example ZnO NR arrays [60], single crystalline GaN NR [61], GaP NR [62] can serve as an effective anti-reflection coating because of their regular textures and morphology. Strontium metaniobate ($SrNb_2O_6$) NT morphologies were proven to be effective photocatalysts when compared to their micro-sized powders. On the other hand, single crystalline ZnO shows enhanced electron collection efficiency than that of polycrystalline ZnO nanostructures [17] due to the shorter collection times of the former. The reflection of light would increase the ratio of non-diffusive absorption and diffusive scattering which results in reducing the photon harvesting [63]. The periodic nature and its intrinsic property of low reflectivity are applied on the NWs as well. NW arrays depict higher theoretical absorbance at lower wavelength regions when compared to their thin film counterparts [64]. The single crystal Si NWs have shown delayed recombination and higher optical absorption [43, 65, 66].

NW structures can absorb the incident photons while the low energy photons are scattered inside the structure. Further increase in the absorbance can be obtained by tailoring the filling factor (FF) of NW [64]. This phenomena of multiple reflections inside the nanostructure is similar to NTs where multiple reflections and scattering takes place within the tube cavity [67]. Furthermore these 1D structures (NWs and NTs) act as electron pathways (like express way) in the axial directions. However, the scattered or transmitted light possesses higher wavelength which forces us to employ sensitizers such as dyes (Eosin-Y [68] in combination with CNT) to increase the η. The arrays of NWs [69] and dual diameter germanium nanopillars [70] depicted effective photon absorption at low (300-600 nm) and high wavelengths (600-900 nm) respectively. Single crystalline TiO_2 NWs showed faster electron mobility (~1 cm^2/Vs) than those of polycrystalline NW [71], likewise single crystalline ZnO NWs (1-5 cm^2/Vs) [72]. Although the mobility of the charge carriers in 1D polycrystalline TiO_2 is comparable to that of 0D TiO_2 [67, 73], the recombination time of the former is much longer than the latter. This may be because of the unevenly distributed recombination centres on the surface. Furthermore, radial electric field that may be present in 1D NWs delays the recombination process which is accounted for the enhanced electron collection efficiency in 1D TiO_2 [73-75]. 1D materials with relatively smaller E_g have shown an η of 0.6 % (branched CuO NW) and 0.71 % (CuO/ZnO core–shell NR arrays) [27]. Hexagonal Zn_2GeO_4 NRs show the highest rate of H_2 evolution[76] of 0.6 $mmol/h^{-1}$. A comparative study was also proves that the Zn_2GeO_4 NRs could produced a stable H_2 evolution rate of 6.24 $mmol/g^{-1}.h^{-1}$ under UV light irradiation[77]. Hematite (α-Fe_2O_3) was considered for the PEC solar water splitting [78] with the 3D nanophotonic structures which resulted in a current density as high as 3.05 mA/cm^{-2} at 1.23 V with respect to the reversible hydrogen electrode (RHE). Hwang et.al., [79]reported that the layered perovskites loaded with nickel are significant photocatalysts for overall water splitting with a photon yield of 23%. However, the quantum yield as high as 30% was obtained when $K_2La_2Ti_3O_{10}$ was prepared by the polymerized complex method[80]. Zhang et.al.,[81] suggested an improved photochemcial H_2 evolution from the TiO_2 leaf structure.

Therefore nanostructures are potential candidates for the water splitting with recyclable properties [82]. Analysis from ISI Web of science has shown extensive growth on the research of H_2 production with an enormous number of publications (Fig. 2). From Fig. 2 and Fig.3, it is clear that PEC water splitting is a potential method to produce H_2 which encompasses environmentally compatible features. Furthermore, analysis of Fig. 3 suggests that the nanostructured materials are promising PEC catalysts.

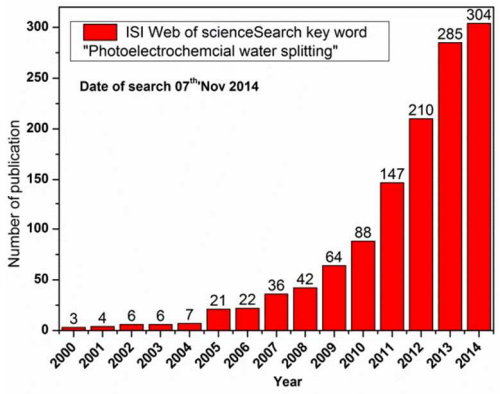

Figure 2: Number of publications against year on photoelectrochemical water splitting.

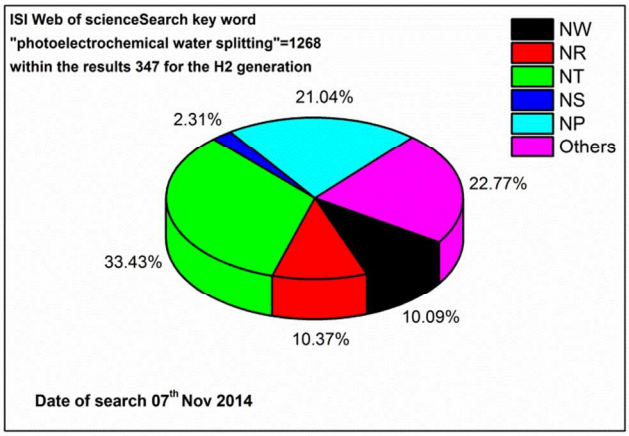

Figure 3: H_2 evolution from various nanostructures via photoelectrochemical water splitting; NW:Nanowires, NR:Nanorods, NT:Nanotubes, NS:Nanosheets, NP:Nanoparticles and Others includes nanofibers, nanolayers, nanoribbons, nanospheres etc.

The present review focuses on the fundamental properties of the nanostructured materials and their efficiency in the context of

processing parameters. The basic mechanism of H_2 evolution is addressed which includes vital points those influence the catalytic activity. Wide range of photocatalysts were developed for their use under UV illumination. They were subjected to modification to extend their capability of utilizing visible light. H_2 evolution from various nanostructures are classified into two major sections *viz* UV and visible illumination along with various types of nanostructures such as NRs, NSs etc. The efficiencies and quantities of H_2 evolution from various materials in different morphologies are tabulated for both UV and visible regions separately. Apart from these, important results and relevant configurations (eg. heterojunctions) are discussed elaborately. In the concluding remarks, we have discussed the crucial points those require further attention which assist in designing the next generation catalysts.

2. Basic mechanism for hydrogen generation

The basic PEC setup [12] of water splitting is shown in Fig.4a, when the electrolysis takes place water molecules undergo redox reactions to generate H_2 and O_2 at Pt and TiO_2 electrodes respectively. This PEC setup was later simplified employing semiconducting particles and/or powders by Bard [13-15] in the presence of aromatic compounds as shown in Fig. 4b, where heterogeneous catalysis was the main aim. In any case involvement of a semiconductor (catalyst) is essential from which the photogenerated *e/h* pairs take part in catalysis. In the light of basic mechanism (discussed in a separate section) the crucial point to enhance the productivity is to delay the recombination of excited *e/h* pairs and subsequent migration (diffusion) to the surface. The output from the catalyst depends on how efficiently *e/h* pairs are created and how well they diffuse to the surface. These factors depend on the semiconductor [16, 17, 60-62], morphology [16, 60], crystal structure [17, 25, 61, 62], defects, intrinsic carrier life time, collection time [17] etc. Interestingly the above mentioned factors can be well tuned in the catalyst when it is in nanodimension. The essential criteria and mechanism of water splitting is as follows. The water molecules are reduced to form H_2 and oxidized to form O_2. Reduction and oxidation are mediated by electrons and holes respectively, where the redox potential of water is 1.23 V, i.e. H^+/H_2 is 0 V and O_2/H_2O is 1.23 V with respect to NHE (see Fig. 4c). Under suitable illumination, electrons and holes are created in CB and VB respectively. In the process of photocatalytic water splitting several factors are involved which determine the η finally. They are (a) absorption of photons to form excited *e/h* pairs, (b) recombination, separation, migration, trapping and migration excited charge carriers and (c) surface chemical reactions (construction of surface reaction active sites for H_2 and O_2 evolution). When the conditions are favorable, these photoexcited electrons and holes migrate to the surface of the photocatalyst as shown in Fig. 4. Fig.4c describes the role of SRs in the process of catalysis. As the quantity of SR decreases so does the H_2 production rate, however the production rate can be retrieved if the reagent is replenished [83]. It was reported that the SRs can effectively reduce H_2O to H_2 or oxide it to O_2. Co-catalyst and/or addition of SRs to TiO_2 evidenced an improved performance [24]. In addition a sufficiently negative flatband potential, good absorption cross section over a wide spectral range, photostable, and an appropriate band gap are essential. In this context metal oxides such as TiO_2, $SrTiO_3$, and $NaTiO_3$ heavily explored because of their suitable band structures, low environmental impact and toxicity and high stability.were However, such wide band gap oxides provide low conversion efficiencies as they are only active under UV light which accounts for just ~4% of the solar spectrum. Buhler et.al [84] reported that CdS is a promising absorption up to 520 nm and its flat-band potential lies at -0.66 V (pH 7). However, the E_g of the CdS is still relatively large (2.5 eV) and not stable in aqueous solution under irradiation (anodic dissolution). Having said that CdS can be stabilized in aqueous solutions by employing reducing agents or SRs which provide electron donors to consume the photogenerated holes. On the other hand, SRs promote H_2 evolution *via* contributing to the half of the reaction[84]. However, employing SRs has two outputs one of which is H_2 while desulfurization processes containing S^{2-} and SO_3^{2-} is very attractive. In the case of dye-sensitization [85] excitation and subsequent charge transfers occur within a sub-nanosecond or picoseconds time scale. Since electrons populate the CB, their energy should be more negative than the H^+/H_2 with reference to NHE. While holes participate in the catalysis from VB, their energy should be more positive than O_2/H_2O (1.23 V) with reference to NHE. Therefore, the E_g of the photocatalyst should be greater than 1.23 eV. Furthermore, the energetic level of CB and VB play a vital role in water splitting where VB and CB edges correspond to the ionization potentialand electron affinity respectively. See Fig. 5, for various semiconductors and their CB and VB edges with reference to NHE and vacuum while the values are tabulated in Table 1 for easy reference.

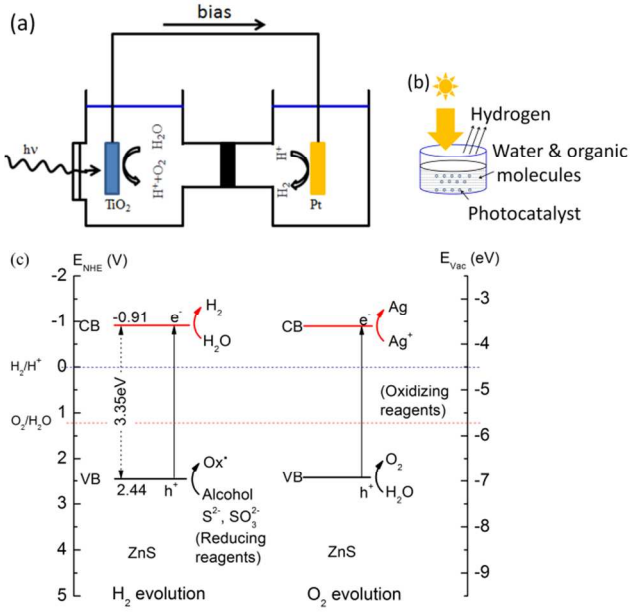

Figure 4: Schematic diagram of the setup for electrochemical water splitting (a) after Ref. [12] (b) powdered photocatalyst after Ref. [13-15] and (c) basic principle of water splitting with photocatalyst materials, figure redrawn based on Ref. [24]

In the following the basic half equations which form H_2 and O_2 gases were given. Due to the uphill nature of the reaction (positive change of Gibbs free energy, ΔG^0= 237 kJ/mol at 25°

C), backward reactions may take place between H_2 and O_2 to form water in addition to intermediates. Hence the surface of the catalyst or co-catalyst (in case if any) should be less supportive to the backward reactions.

Reduction-Pt (Fig.4c): $2H^+(aq) + 2e^- \rightarrow H_2(g)$ (1)

Oxidation-catalyst (Fig.4c): $2H_2O(l) + 4h^+ \rightarrow O_2(g) + 4H^+$ (2)

Overall reaction: $2H_2O(l) \rightarrow 2\,H_2(g) + O_2(g)$ (3)

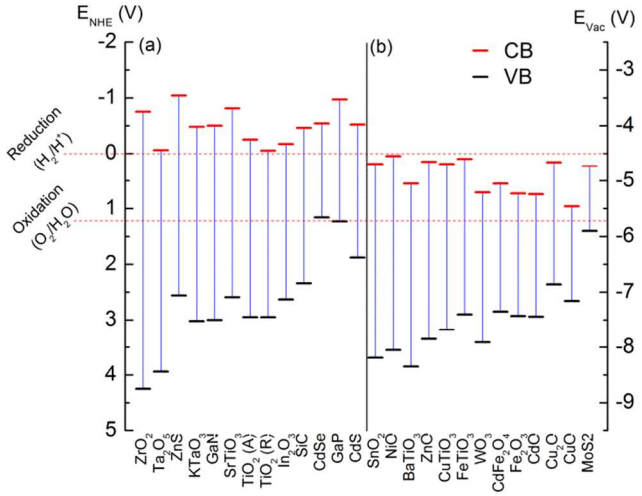

Figure 5: Absolute conduction band and valance band energy levels for some semiconducting photocatalysts with respect to normal hydrogen electrode (NHE) and vacuum (Vac). Thermodynamically (a) suitable and (b) unsuitable materials. Please consult Ref. [86] for the band edge values for various other perovskites.

Table 1: The VB and CB levels of some semiconductors.

Semiconductor	Band levels with respect to NHE (eV)			Ref
	CB	VB	E_g	
ZrO_2	-0.75	4.25	5.0	87
Ta_2O5	-0.06	3.94	4.0	87
ZnS	-0.91	2.44	3.35	88
$KTaO_3$	-0.48	3.02	3.5	87
GaN	-0.5	3.0	3.5	89
$SrTiO_3$	-0.81	2.59	3.4	90
TiO_2(A)	-0.25	2.95	3.2	90
TiO_2 (R)	-0.05	2.95	3.0	90
In_2O_3	-0.17	2.63	2.8	87
SiC	-0.46	2.34	2.8	91
CdSe	-0.54	1.16	1.7	24
GaP	-0.97	1.23	2.2	24
CdS	-0.52	1.88	2.4	87
SnO_2	0.19	3.69	3.5	87
NiO	0.05	3.55	3.5	87
$BaTiO_3$	0.55	3.85	3.3	87
ZnO	0.15	3.35	3.2	87
$CuTiO_3$	0.19	3.18	3.0	87
$FeTiO_3$	0.1	2.9	2.8	87
WO_3	0.71	3.41	2.7	87
$CdFe_2O_4$	0.55	2.85	2.3	87
Fe_2O_3	0.73	2.93	2.2	87
CdO	0.74	2.94	2.2	87
Cu_2O	0.16	2.36	2.2	87
CuO	0.96	2.66	1.7	87
MoS_2	0.23	1.4	1.2	87

Fig. 5 consists of two parts ,(a) and (b) which are suitable and unsuitable materials for H_2 production, respectively. If we look at Fig. 5a, we can see that for most of the semiconductors the VB edge is deeper than O_2/H_2O oxidation potential. Hence there is no requirement of co-catalyst, except for special cases. As mentioned in the introduction, to increase η one should try to use the visible light of the solar spectrum. Although there are some semiconductors whose band gap lies within the range of solar visible light, because of their unsuitable band energies with respect to NHE they are not considered as active materials. They are known to be photocorrosive materials e.g. MoS_2, Fe_2O_3, WO_3 etc where their CB minima is lower than thermodynamic requirement (Fig. 5b) [24]. On the other hand wide band gap materials cannot harvest the visible light, unless suitably modified. As an example, we have shown a schematic diagram for doped TiO_2 in Fig. 6 [34]. In the case of UV-illumination ($h\nu_1$) H_2 and O_2 evolution are favorable. In the S-doped TiO_2 the evolution of O_2 is possible at S^{2-} site under visible light illumination ($h\nu_2$), i.e. S^{2-} state lies above the O_2/H_2O oxidation potential. On the contrary, in the case of V-doped TiO_2, evolution of H_2 is not possible at $V^{4+/5+}$ site under visible light illumination ($h\nu_3$), i.e. $V^{4+/5+}$ state is at higher potential than H_2/H^+ reduction value. It is very important to note that the dopants form localized states. If they are accessible on the surface then catalysis takes place from hole and electron if the redox potentials' essential criteria are met. If they are not physically present on the surface then under visible light illumination *e/h* pairs are created, however, electron or hole take part in catalysis for S and V dopings respectively. Over the past few decades many photocatalysts have been reported to work under UV/Visible/light irradiation [2].

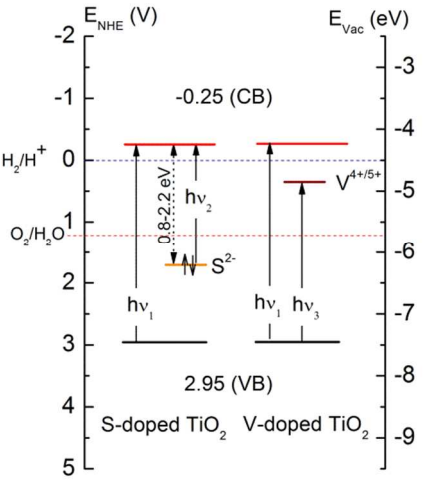

Figure 6: Schematic band diagram for S or V doped TiO_2. Figure redrawn on the basis of Ref. [34].

To continue discussion on the influencing factors, charge separation and migration of photogenerated charge carriers are strongly affected by the change in crystal structure (polymorphs) [77, 92], crystallinity [93] and particle sizes. The defects in the lattice act as traps or recombination centers and consequently the catalytic activity decreases. The density of defects can be lowered by increasing the crystallinity. By decreasing the size of the semiconductor, the photogenerated *e/h* pairs can migrate to the surface before being trapped or recombined. If the catalytic site is not available even after reaching the surface, then they will have to recombine irrespective of the fact that they have high enough potential to split the water. The surface chemical reactions depend on the SA and the density of surface defects.

Earlier it is seen that the doped TiO_2 can be visible active where the dopants create intermediate bands within the band gap. However, in a special scenario H_2 evolution varies within the polymorphs of TiO_2 [92] (Fig. 7), where the flat band potential of rutile and anatase vary with reference to H^+ reduction potential. i.e. flat band potential of rutile TiO_2 is almost the same as that of reduction potential of proton, while that of anatase TiO_2 is shifted negatively by ~0.2 V [94]. This implies that photogenerated electrons in anatase are more energetic than that of rutile. When the recombination sites are predominant, like in the case of amorphous TiO_2, one can expect negligible catalytic activity [95]. Another polymorph of TiO_2 is brookite which has shown better catalytic activity than commercial TiO_2 (P-25) [96]. Again the difference in the flat band potential (for brookite it is 0.14V cathodically shifted than that of anatase) is the reason for higher efficiency. Kandiel et.al.[92] have studied three types of TiO_2 polymorphs for H_2 production from MeOH-H_2O vapors. The results suggest that anatase and brookite phases depicted similar H_2 production, while rutile has shown the lowest performance. Cubic structured $KNbO_3$ depicted higher rate of H_2 production among orthorhombic and commercial $KNbO_3$ [97].

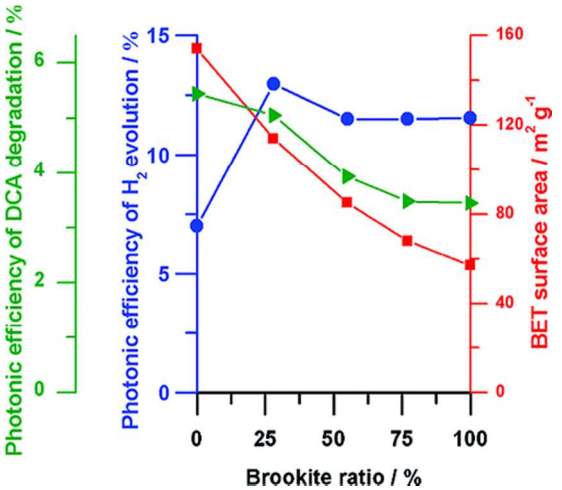

Figure 7: Photonic efficiency versus surface area and the content of brookite. Triangle-photonic efficiency of dichloroacetic acid (DCA) degradation, square-surface area and circle-photonic efficiency of H_2 evolution. Conditions: 0.5 g/L catalyst, 60 mL of aqueous 1 mM L-1 DCA and pH is 3 Ref. [92].

3. Quantification of hydrogen generation

Researchers employ many types of illumination sources (Xe lamp, Hg lamp etc) at different catalyst quantities. In order to understand the current state of art one needs a well agreeable quantification method so that the efficiency can be compared across many different studies. In this section we have given those methods.

Solar to hydrogen conversion efficiency (η %): The efficiency of H_2 generation can be measured either by quantifying the amount of H_2 gas evaluated or electrons transferred from photocatalyst to water within a certain time period under illumination. The overall solar energy conversion is given by the following equation [33].

$$\eta\ (\%) = \frac{total\ power\ output - electrical\ power\ output}{energy\ of\ incident\ light} \times 100$$

$$= j_p\left[\left(E^0_{rev} - |E_{app}|\right)/I_O\right] \times 100 \qquad (4)$$

where j_p is the photocurrent density (mW/cm^2), $j_p\, E^0_{rev}$ is the total power out put, $j_p|E_{app}|$ is the electrical power output, and I_0 is the power density of incident light (mW/cm^2). E^0_{rev} is the standard reversible potential (1.23 V/NHE). E_{app} is the applied potential which can be derived from $E_{app} = E_{meas} - E_{aoc}$, where E_{meas} is the electrode potential of the working electrode at which photocurrent was measured under illumination and E_{aoc} is the electrode potential of the same working electrode under open circuit, under the same illumination when immersed in the same electrolyte. E_{aoc} and E_{app} are measured with respect to Ag/AgCl. The voltage at which the photocurrent becomes zero was taken as E_{aoc}. Furthermore the details of light source can be included in the quantification process and quantum yield (QY) can be calculated. The overall QY is defined for H_2 and O_2 in equations (5) and (6) respectively[98].

$$QY\% = \frac{2 \times Number\ of\ evolved\ H_2\ molecules}{Number\ of\ \text{absorbed}\ photons} \times 100 \quad (5)$$

$$QY\% = \frac{4 \times Number\ of\ evolved\ O_2\ molecules}{Number\ of\ \text{absorbed}\ photons} \times 100 \quad (6)$$

As see earlier some of the photocatalysts are active in visible while the other in UV region of the solar spectrum. Although the principle of H_2 generation is the same for both UV and visible irradiations, by given the large amount of visible light availability it would be appropriate to discuss them separately. Therefore we have divided the studies based on their illumination regions such as UV and visible while all the types of nanostructures are discussed for each category.

4. UV-active nanostructured photocatalysts for hydrogen generation

Earlier we have seen that wide band gap semiconductors can utilize the UV region of the solar spectrum only. Nevertheless, considerable quantities of H_2 has been produced [47-52] in the literature when the catalysts were in the form of nanostructures [5, 99]. To emphasize, the density of active sites on the surface increases with increasing SA [100-102], especially the case with 1D nanostructures which have fast charge transfer and efficient charge separation [103]. For example, nanowires [93, 104, 105], nanotubes [106-110], nanorods/nanoribbons [111-116] and nanofibers [44, 117-121] have depicted great potential for H_2 production. However, it is vital to understand which type of 1D structure is more beneficial for H_2 energy generation. Hence in the following we have comparatively analyzed these 1D structures against their efficiency under UV irradiation.

4.1. Nanowires

NWs have shown significance photocatalytic activity due to improvement of electron-hole separation and lower recombination rate. Such remarkable features are in fact highly desirable to enhance the efficiency of the PEC water splitting. NWs have been extensively studied in the recent literature[93, 122-124]. Yang et.al [122] reported that the N-doped ZnO NWs as photoanodes in PEC yielding relatively higher efficiencies because of the improved charge transport over 0-D nanostructures. TiO_2 NWs were proven to be effective for the H_2 generation than commercial TiO_2 nanoparticles (NPs). They yield was ~1.421 μmol/m^2 which is quite significant [123] and ascribed to the high SA and low recombination rate of *e/h* pairs. Jitputti et al.,[93] studied TiO_2 NWs with methanol as SR to unveil the effect of post treatment and its consequence on SA. The SRs are of course remove the photogenerated holes in an irreversible fashion, thereby preventing the mutual electron-hole recombination and H_2 and O_2 back reaction [124], see equation (2). The overall process can be expressed by the following equation [125]:

$$CH_3OH \xrightarrow{hv,Cat.} HCHO + H_2 \quad (7)$$

$$HCHO + H_2O \xrightarrow{hv,Cat.} HCO_2H + H_2 \quad (8)$$

$$HCO_2H \xrightarrow{hv,Cat.} CO_2 + H_2 \quad (9)$$

$$CO_2 + H_2O \xrightarrow{hv,(M-TiO_2)} \begin{cases} CH_4 \\ CH_2O \\ CH_3COOH \\ (where\ M = Pt, Pd, Au, Cu, Ru) \end{cases} \quad (10)$$

Notably methanol is oxidized to form CO_2 which is an adverse effect. Despite the H_2 yield is ~20.1 μmol h^{-1} for the samples which were post treated at 500 °C for 1h (Fig. 8). This may be because of the unique 1D NWs and high crystallinity could have promoted the H_2 evolution under UV irradiation [93]. The amount of H_2 increases with increasing post treatment temperature until 500 °C, then its starts decreasing with further increase in temperature. The decrease might be due to lowered SA. Similar effect is reported [26] for lithium niobate ($LiNbO_3$) NWs where higher SA yielded better results. On the other hand when RuO_2 is employed as a co-catalyst under UV-Vis illumination, the overall water splitting is increased.

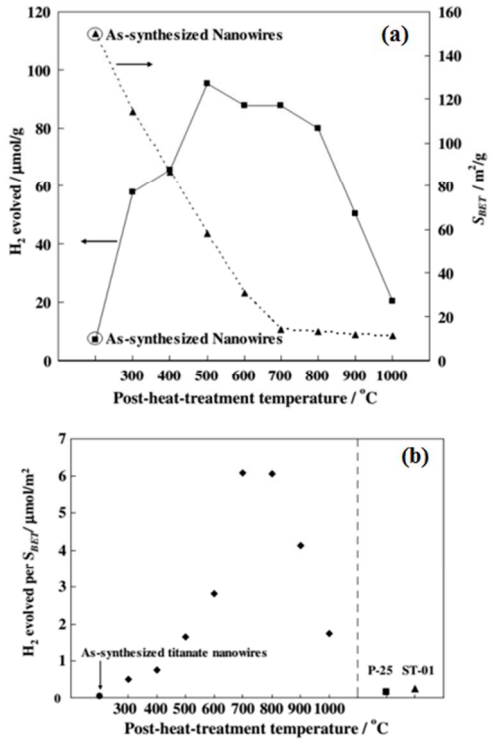

Figure 8: H_2 generation efficiency with respect to post-treatment temperatures on (a) surface area (S_{BET}) and (b) TiO_2 powder (Degussa P-25) and commercial TiO_2 (Ishihara ST-01)[93]

Si NWs (*n*-type) are known for their competitive carrier recombination. As outlined in section 1.1, forming a *pn*-heterojunction in fact accelerates the separation of photogenerated charge carriers. This is shown by employing Cu_2O (*p*-type) as core-shell structure with Pt as co-catalyst as shown by Xiong et al., [59]. This composite structure has demonstrated nearly 45 % increase in the H_2 generation when compared to pristine Si NWs. In contrast to *pn*-type, [59] *nn*-type heterojunctions were also a subject of investigation in a similar core-shell structure with ZnO-$Zn_xCd_{1-x}Te$ NWs [35]. Contextually, it is vital to point out a study [36] in which the authors have shown that selective isolation of electron hole pair in a *nn*-type heterojunction. Such structures help to isolate the hole thereby inhibiting the back reactions. In ZnO/$Zn_xCd_{1-x}Te$ NWs heterojunction the shell materials absorbs in NIR region (855 nm) in contrast to the core which absorbs UV region (380 nm) covering ~22% of solar spectrum. Under suitable illumination, type-II band alignment allows transfer of photogenerated electrons from the CB of $Zn_xCd_{1-x}Te$ (E_g tunability 2.25 to 1.45 eV depending on the Cd, Zn ratio) to the CB of ZnO (Fig. 9a). The recombination is delayed while being transferred yielding higher H_2 production. The electrons collected at ITO produce H_2 molecules. On the other hand, the holes are transferred to the VB of the $Zn_xCd_{1-x}Te$ shell and consumed by the SR (S^{2-} and SO_3^{2-}). It is vital to note that in the process of the fabrication if

$Zn_xCd_{1-x}Te$ covers the whole substrate including ITO, then it is not useful for H_2 generation. ITO being an expensive substrate, alternative methods should be considered. For example, if ZnO is taken as shell and $Zn_xCd_{1-x}Te$ as core, then the electrons can take part in catalysis from much higher SA (in the original configuration [35] it is just ITO). Furthermore, even if the ZnO covers the whole substrate a good access to electrons is preserved where the fabrication difficulties in this configuration are acknowledged.

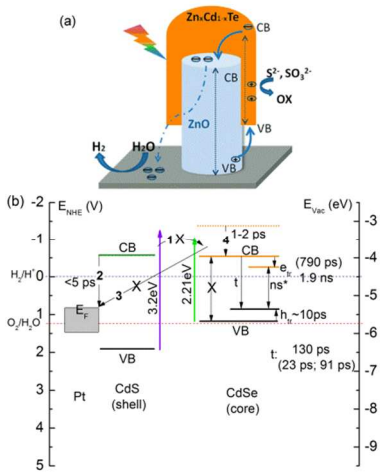

Figure 9: (a) Schematic representation of charge transfer and separation process in ZnO/$Zn_xCd_{1-x}Te$ core/shell NW array [35], (b) CdSe/CdS core-shell NWs heterojunctions with Pt as co-catalysts [126]. e_{tr} and h_{tr} are electron and hole traps respectively.

These heterojunctions are further developed by introducing Pt as co-catalysts [126] for example, CdSe/CdS core-shell NWs heterojunction. After charge generation Pt acts as an electron collector and enhances the H_2 production at its best value of 434.29 μmol h^{-1} g^{-1} under UV illumination. The CdS shell also helps to passivate the surface defects of core which helps to increase the carrier life time. In Ref. [126] the authors have illustrated the band diagram without considering the energetic locations of the bands. However, we have redrawn and depicted in Fig. 9b, where the CB and VB edges for the two semiconductors are taken from table 1. In process 1 the authors [126] suggest that the electron from CB of CdS doesn't to reach CB of CdSe. In process 2 electron from CB of CdS takes < 5ps to reach the E_F of Pt. Process 3 is of course not possible by given the physical inaccessibility. In process 4 electron takes nearly 1-2ps to reach the bottom of the CB of CdSe. Electron and hole trap processes (e_{tr}, h_{tr} respectively) take place in CdSe and the time scales are given on Fig. 9b. Within CdSe the authors also suggest that the electrons are not excited to the bottom of CB and hence do not recombine directly, however mediated by e_{tr} and h_{tr}. Wu et al., [127] reported H_2 evolution from nitrogen doped TiO_2 NFs (hydrothermal) decorated with Pt NPs of ~2 nm diameter under different illumination wavelengths. The catalysts were found more effective in production of H_2 exhibiting conversion efficiencies of 3.6 % and 12.3 % for 365 nm and 312 nm of UV irradiation, respectively.

4.2. Nanotubes

TiO_2 based NTs demonstrated considerable η under UV irradiation in recent years [33, 128-132]. The physical dimensions of these NTs are the factors those control the efficiency of overall water splitting. When the scattering of the light increases within the structure higher rate of H_2 generation can be expected where flat electrode have shown less absorption [129]. Paulose et.al.,[33] fabricated self-aligned TiO_2 NTs (134 μm length, 20-150 nm pore diameter) by anodization where the process parameters allow the tunability of the pore size and length (Fig. 10a to c). After annealing the amorphous NT at 550 °C the photoconversion efficiency of ~16.25 % was achieved under UV illumination. Mor et.al., [128] demonstrated the Ti−Fe−O NTs based thin films with H_2 production rate of ~7.1 mL/Wh. Eder et.al [133] reported Fe/Pt–TiO_2 NTs possessing superior electron life time and efficient charge separation under UV light [131, 134]. As mentioned earlier, the bulk recombination is reduced by the NT architecture (porosity) while the photogenerated minority carriers (holes) can be trapped by surface states according to a model proposed by Lubberhuizen et al.,[135]. For example a typical time needed for holes to reach the surface is ~10^{-10} s in nanoporous GaP.

It is known that noble metals (Au [136, 137], Pt [46, 133, 138], Ag [139], Pd [140] etc) and many co-catalysts (NiO_x [46] etc) act as electron reservoirs (acceptors) [138] where they collect the photogenerated electrons from CB of semiconductor under intimate contact. As a result the recombination is delayed, i.e. Fermi level (E_F) equilibration of metal and semiconductor. As expected the delayed recombination helps to enhance the activity of the catalyst. Furthermore Pt is very special because of the following reasons. (a) Favorable H^+ chemisorption energy and high activity for proton reduction reactions, (b) low electrochemical impedance to discharge the absorbents [138] etc. Please refer to the cross references in Ref.[126] Furthermore, Pt forms Schottky junction with TiO_2 which is crucial for H_2 generation. However when c calcined at 873 K the formation of Schottky barrier is prevented. [141]. As an addition advantage, these noble metals are not photocorrosive. On the other hand an optimum loading Pt should be maintained. Excessive loadings can decrease the H_2 production because of the decreased SA for chemisorption [142, 143]. In the context of Au the performance depends on the shape and structure [137].

TiO_2 NTs with Au NPs have shown enhanced the H_2 production [136]. Pd quantum dots (QDs) are employed in conjunction with TiO_2 NTs in a solution containing Na_2CO_3 and ethylene glycol (EG) and the results were significant [140]. SEM images of TiO_2 NTs array with Pd QDs are shown in Fig. 10a to c, H_2 evolution is shown in Fig. 10d [140]. The measurements are performed at −0.3 V standard calomel electrode containing 2 M Na_2CO_3 + 0.5 M EG solution under 320 mW/cm^2 irradiation for Pd weight percentage of 2.15. Pt NPs were extensively employed in conjunction with TiO_2 NTs [144] reporting a QY of ~16% under UV irradiation.

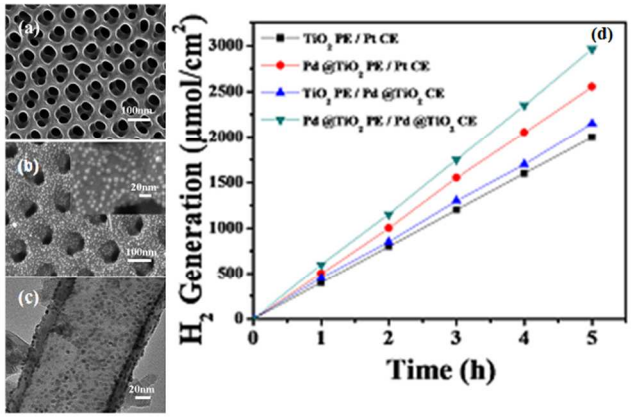

Figure 10: SEM micrographs of (a) TiO_2 NTs (b) Pd QDs coated TiO_2 NTs, inset shows higher magnification, (c) TEM image of TiO_2 NTs with Pd QDs and (d) H_2 generation from various catalysts against time [140].

The recombination rate of *e/h* pairs in TiO_2 NTs is reduced in the presence of Ag NPs(Fig. 11a-c). Interestingly, the yield of H_2 (~10.69 µmol/h) is dependent on anodization voltage and time (texture of TiO_2 NTs) [139], see Fig. 11d and e. In the present context smooth texture provide a better channel for the transport of electrons with minimal scattering. Similar results are reported by Li et al. [145] where morphology, anodization potential and time were interlinked with the H_2 production efficiency.

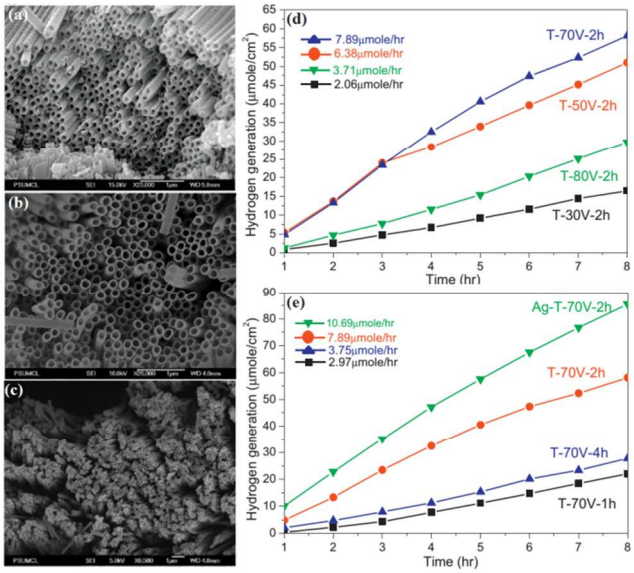

Figure 11: FE-SEM images of NT arrays by anodization at (a) 60 V, 0.25 wt% NH_4F in ethylene glycol (b) 40 V, in dimethyl sulfoxide (DMSO) with 2% of HF, (c) 60 V, in DMSO containing 2% HF [33]. The H_2 generation measured from (d) TiO_2 NTs produced from different anodization voltages and (e) the Ag modified TiO_2 NTs and unmodified NTs with respect to anodization time [139].

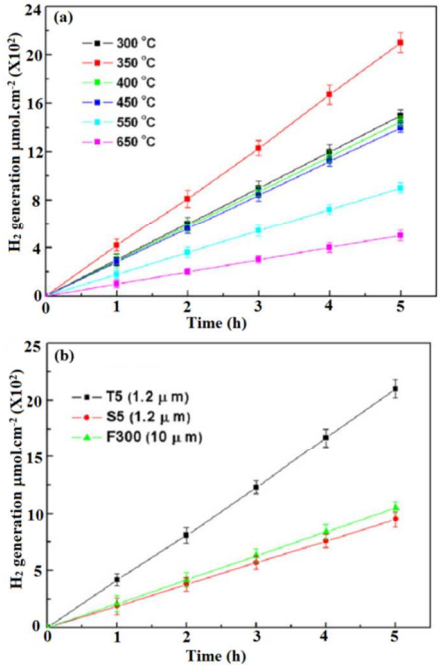

Figure 12: The amount of H_2 generated from catalysts produced (a) at different annealing temperatures (b) by highly ordered TiO_2 NTs in the first (F300), second (S5) and third (T5) anodization [146].

To continue the discussion on the process parameters of TiO_2 NTs an annealing temperature of ~350 °C is found to be optimum [146]. At higher annealing temperatures, the barrier thickness of NT arrays and Ti substrate gets thicker which inhibits the transfer of charge to the Ti substrate. The corresponding H_2 generation with respect to the temperature and cycle times is shown in Fig. 12. W doped (W^{6+} state) TiO_2 NTs were investigated under glycerol/fluoride electrolyte and the production of H_2 was about 24.97 µmol/h which depends on W loading and annealing temperature [147]. The effect of processing parameters extends to Ta_2O_5 NTs where an investigation by Goncalves et al. [148] suggest that the anodization potentials, electrolyte temperature (diameter, length of NTs) and annealing temperature influence the H_2 generation with ethanol as SR. Figure 13 depicts the current densities at different electrolyte temperatures from which the variation of length and diameter of the tubes can be seen. Goncalves et al. [148] observed CO, CO_2, CH_4, C_2H_4 and C_2H_6 gases were observed in the process of ethanol photo-reformation. It is interesting to see that the amount of gases generation also increased with increasing annealing temperatures [148]. Single crystalline NT arrays of $SrNb_2O_6$ with rhombic cross sections exhibited superior H_2 evolution than their bulk counterparts because of smaller diffusion length of the charge carriers apart from high SA [46]. This was further enhanced (to 102 µmol/g) by introducing NiO_x and Pt by impregnation and photodeposition methods, respectively.

H_2 production efficiencies can be enhanced by carbon rich catalysts such as graphene, multiwalled carbon nanotubes (MWCNTs), carbon fibers, activated carbon etc. Cargnello et.al [149] enhanced H_2 generation from MWCNTs@M/TiO_2 of ~10 mmol $h^{-1}g^{-1}$ in the presence of methanol as SR, where M = Pt or Pd. It is also suggested that the nanocomposite with Pt was slightly more active than that of Pd. This is because of the various

positive effects from the MWCNT, Pt and metal oxide. Primarily MWCNT can delocalize the photogenerated electrons enhancing the lifetime of the charge carriers which eventually increases the H_2 evolution (also see the Ref.[150]).

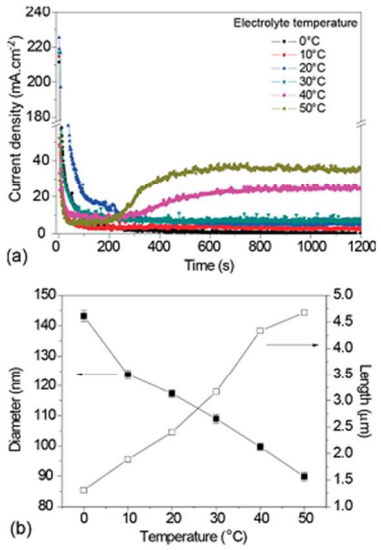

Figure 13: (a) Current density curves for anodization of Ta discs at 50 V at different electrolyte temperatures and (b) effect of electrolyte temperature on the outer diameter and length of the NTs [148].

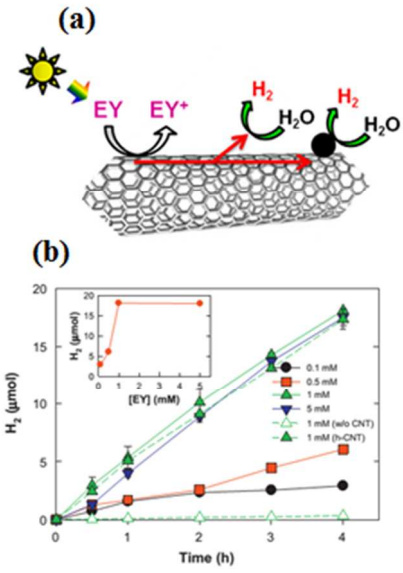

Figure 14: Eosin sensitized (a) CNT-catalyst (b) H_2 production as a function of EY concentration [68].

In a typical investigation [68] eosin-Y(EY) and triethanolamine (TEOA) were used as sensitizer and electron donor respectively, where it is suggested that MWCNTs exhibited nearly 9-fold enhancement in performance among all other carbon rich catalysts under simulated sun light [68]. Schematic representation of EY loaded MWCNT is shown in Fig. 14a on which noble metal NPs can also be employed. H_2 evolution against EY concentration is shown Fig. 14b.

4.3. Nanorods

Arrays of NR carry similar effects to that of NWs like high SA [111, 114], promoting the surface reactions rather than recombination [151], short collection lengths for excited carriers in a direction normal to the light absorption. Rutile TiO_2 NRs demonstrated efficient H_2 generation in aqueous solution containing methanol–water SRs in the presence of Cu^{2+} under UV light irradiation [152]. In addition the design of the radial *pn* junction NR device could provide large improvements in efficiency relative to a conventional planar geometry [153].

$SrSnO_3$ NR structures were synthesized via hydrothermal method and they exhibited better H_2 production rates in comparison with that of dumbbell like structures (Fig. 15a). Figure 15b depicts UV-Vis diffuse reflectance spectra of these NRs and dumbells along with band diagram of $SrSnO_3$ [154].

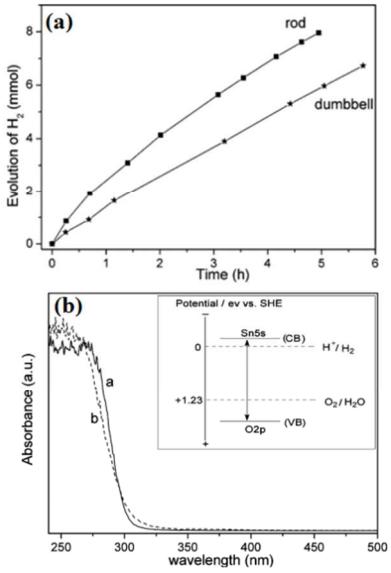

Figure 15: (a) H_2 evolution from $SrSnO_3$ NRs and nanobumbbells (b) UV-Vis diffuse reflectance spectra of $SrSnO_3$ from NR (dot line) and dumbbell-like (solid line) morphology. Inset shows the band diagram of $SrSnO_3$ [154].

In Sun et.al.'s [155] study Sb doped SnO_2 NRs is employed as a transparent electrode in the presence of H_2O_2 SR which improved the conductivity of the scaffold. The improvement in PEC performance is due enhanced charge separation efficiency and charge injection efficiency. Furthermore controlled incorporation of Sn doped TiO_2 NRs achieved good PEC performance[156]. Wang et.al [143], reported that the well dispersed CdZnS single crystalline NRs exhibited higher H_2 generation than CdS where the aqueous solution contains two different SRs (SO_3^{2-} and S^{2-}) with and without Pt under simulated solar light. The enhancement is attributed to the abundant hydrogen reactive sites on CdZnS. However, incorporation of SRs, co-catalyst, sensitizers, electrolytes and reducing agents yielded better performance [144]. While the affecting parameters in catalytic activity of SRs are not yet well understood. Higher activity is associated with proton exchange capability of the material. Sometimes the native

material itself performs better even in the absence of co-catalysts. Nanostructures of Zn_2GeO_4 have been studied in the literature on several occasions[25, 76, 77, 157, 158]. Liang et.al., [76] reported on hexagonal Zn_2GeO_4 NFs and NRs (Fig. 16a, b) and compared the H_2 evolution with its bulk counterpart (Fig. 16c). The results suggest that Zn_2GeO_4 NRs have shown better H_2 evolution than NFs and bulk particles where the NRs have shown predominant reflections from (110), $(2\bar{1}0)$, $(1\bar{2}0)$, $(\bar{1}\bar{1}0)$, $(\bar{2}10)$ and $(\bar{1}\bar{2}0)$ planes. Another study on Zn_2GeO_4 suggests that rhombohedral phase crystal orientation yields better H_2 evolution [77]. Similar to TiO_2 nanostructures the process parameters of Zn_2GeO_4 play a crucial role in determining the efficiency of catalytic H_2 generation. Lin et. al., [157] studied H_2 evolution on the calcination temperature of Zn_2GeO_4 NRs. The results (Fig. 17) suggests that higher calcination temperature (1000 °C) has shown a performance as high as 430 $\mu molh^{-1}g^{-1}$ which is nearly seven times higher than that of a sample calcined at 400 °C [157]. On the other hand, interestingly, the SA dropped to 1/5th of the sample calcined at 400 °C. Although SA is a factor that influences the H_2 production, the other more crucialparameter is the quality of the crystal and its facets[25, 77]. Yan et. al., [25] reported that Zn_2GeO_4 NRs have shown the best performance with 3 wt% of RuO_2. The overall water splitting depends on synthesis temperature where NRs obtained at lower temperatures (40 °C) gave dominant crystal face (110). This face may induce the strong CO_2 gas adsorption and hence higher H_2 production. See another method suggested by Liang et. al.,[158] for crystal orientation and self assembly of Zn_2GeO_4 NRs.

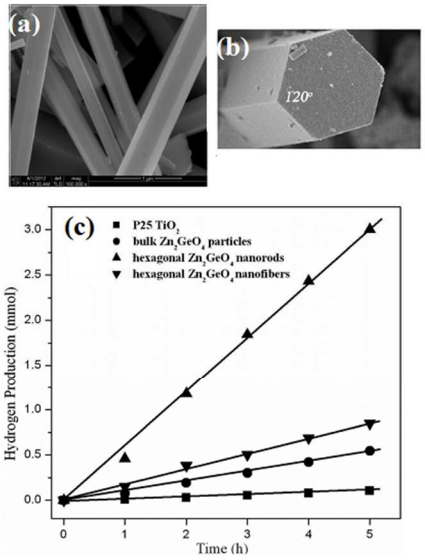

Figure 16: FE-SEM images (a) of the samples obtained at 200 °C at 1.6 g of NaOH concentration, (b) cross sectional view of NF and (c) H_2 evolution rate from an aqueous MeOH solution compared with various photocatalysts under UV light. Catalyst amount 0.1 g; H_2O and CH_3OH volumes are 155 mL and 5 mL, respectively [76].

Again similar to the earlier core-shell heterojunction type catalysts, Yang et.al.,[159] reported on the fabrication of In_2O_3–In_2S_3 core-shell type NRs depicting better performance than individual NR counterparts. The band diagram of the interface of the In_2O_3 and In_2S_3 shell is shown in Fig. 18 where the energetic alignment of the bands favors the transfer of electrons as well as holes to the shell layer (type-I band alignment). It is notable that if electrons and holes are transferred to the shell region. Of course the recombination is delayed yielding O_2 and H_2 which may cause back reaction. Also note the earlier type-II core-shell structure as discussed in Section 4.1.

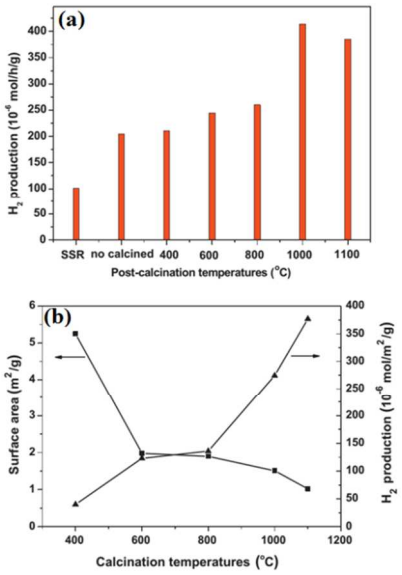

Figure 17: H_2 evolution from Zn_2GeO_4 samples (a) calcined at various temperatures. Conditions: 0.1 g of photocatalyst, 0.1 wt% of Pt co-catalyst, aqueous MeOH solution (100 mL of 20 vol%) and (b) Surface area against calcination temperature [157].

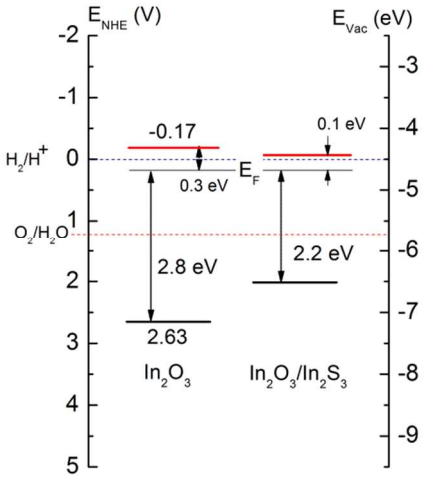

Figure 18: Band diagram of In_2O_3 and In_2S_3 core-shell interfaces. Figure redrawn based on Ref. [159].

4.4. Electrospun Nanofibers

Electrospinning is one of the versatile and convenient technologies to produce 1D nanostructures [160-163] among other physical and chemical fiber synthesis methods [164-169]. 1D nanofibers have proven to be important in electronics, optoelectronics, magnetic sensor [170], photo dye degradation [36, 171-173] photocatalysis[174], and energy harvesting technologies [175-178]. Functional electrospun nanofibers exhibit significant optical [179-

[185] and/or electronic properties [186-197]. In the context of H_2 production TiO_2 electrospun nanofibers (Fig. 19) are found to perform better than the nanostructures produced by hydrothermal synthesis where the process parameter such as calcination temperature, (crystallinity) and SA (Fig. 20) are determining factors [117].

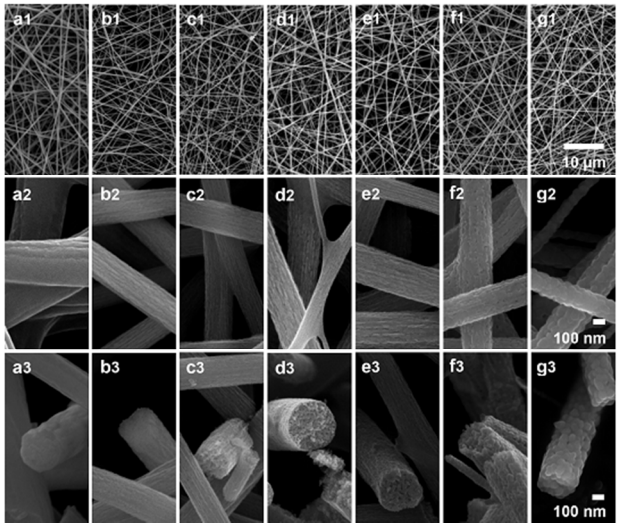

Figure 19: SEM images of (a) as-spun TiO_2 precursor NFs and after calcination at (b) 300 °C, (c) 400 °C, (d) 450 °C, (e) 500 °C, (f) 600 °C and (g) 700 °C for 3 h [117].

The results suggest that 450 °C calcination temperature is optimum for the highest yield. However it is also notable that although 400 °C calcination depicted the highest SAbecause of the lowered crystallinity the H_2 evolution is not significant (Fig. 20b). Similar to NRs and NWs, noble metal NPs are employed in conjunction with NFs which act as electron skin and enhance the H_2 production. See for example, in Zhang et. al.,'s [118] study Au and Pt NPs were employed simultaneously in the presence of SRs (0.1M L-ascorbic acid at pH = 4.0). The results suggest that the best combination is $Au_{0.25}/Pt_{0.25}/TiO_2$ [118]. In Ref. [118] authors suggest that no H_2 evolution is observed for the case of Au NPs under the surface plasmon resonance illumination (~550 nm or visible). The process of electrospinning can be applied to mixed oxides such as TiO_2-SnO_2 [119] and the calcination temperature plays key role in the efficiency of H_2 generation (methanol is employed as SR). Another catalyst combination is $SrTiO_3$-TiO_2 NFs for which the efficiency is better than their individual counterparts where water/methanol mixture is used as a SRs under UV irradiation [198]. Similar to the earlier cases the H_2 yield is dependent on the calcination temperature and SA [120]. These composite fibers are in contrast to that of core-shell type structures where one can smartly choose the material combination so that the transfer of electron to the shell region and hole to the core region takes place. However, in the case of composite structures, the recombination of photogenerated electron and hole is delayed during the transfer while both stay within the structure. Furthermore, the long NF structure and larger specific SA are advantageous for the catalytic activity [121]. Also see an earlier study from our group to produce MWCNT/TiO_2 NFs and their H_2 generation capability [44].

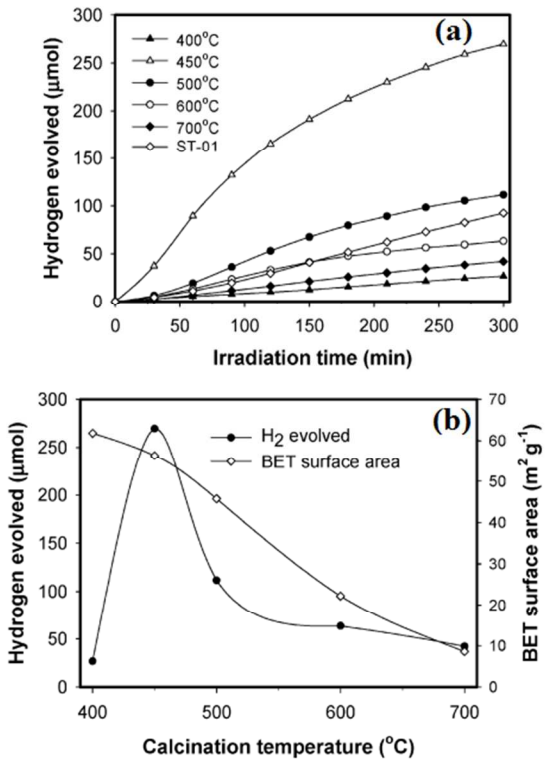

Figure 20: H_2 production (a) with TiO_2 fibers calcined at various temperatures and (b) dependence of the calcination temperature on the BET surface area [117].

4.5. Two dimensional nanostructures

In the previous sections we have seen the 1D materials and their application in the H_2 production. 2D nanostructures such as nanobelts [199-201], nanosheets [202-204], nanoplates [205-207], nanolayers [208, 209], nanoribbons [115, 210] and nanoleaf [211] are also found to be efficient for the H_2 production, where transfer of charge carriers to the surface takes place similar to 1D structures which helps to enhance the performance [201, 212-216].

Pure TiO_2 nanosheet surface is catalytic inactive due to the presence of the large over potential and fast backward reaction (generation of H_2O), while surface fluorinated Pt/TiO_2 nanosheets (NSs) have shown significant catalytic activity [217]. Also note the contradicting study in which TiO_2 ultrathin NSs displayed high catalytic activity due to shorter migration time which suppresses the recombination[218]. The process of generation of photogenerated electrons and holes at TiO_2 surface is shown in Fig. 21a. Pt in this case acts very similar to that of earlier case serving as an electron skin (Fig. 21b). However, an optimum amount of Pt should be determined as shown in Fig. 21c with further increase in the Pt content decreases the H_2 production. TiO_2 NSs exhibited better performance than commercial TiO_2 anatase powder [219] while TiOx NSs by photodepositing metal and metal oxide have shown enhanced activity [203] where *e/h* recombination is slower in the TiOx NSs than single crystalline counterparts. In the case of single crystalline NSs the photogenerated electrons react at the edge of the NSs while in contrast, holes reacts all over the surface.

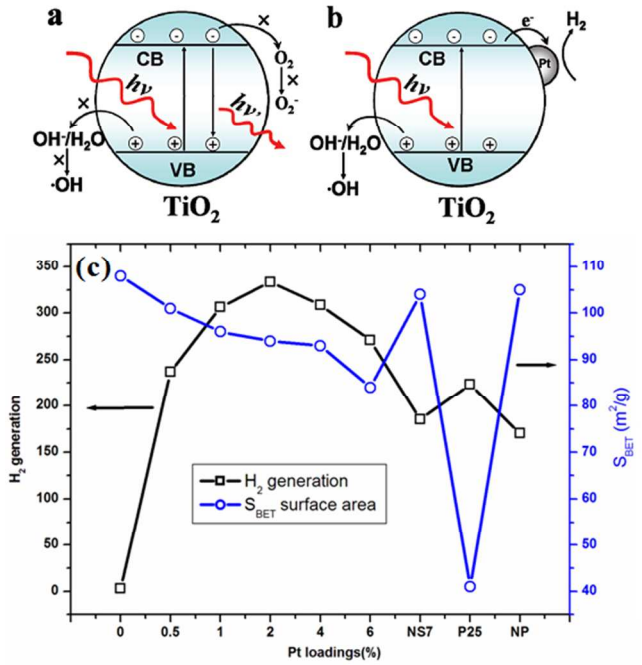

Figure 21: Probable dynamics of photogenerated electrons and holes on the surface of TiO_2 in a clean (a) anaerobic environment, (b) in the presence of Pt [217] and (c) H_2 generation with respect to the surface area and Pt loadings in TiO_2 (fluorinated); NS7 represents without fluorination, P25-degussa and NP: NPs of TiO_2 [217].

ZnO nanobelt (NB) arrays depicted comparatively better activity than thin films or the rod/comb like ZnO nanostructures under similar conditions [199]. Micro and nanocomponents of ZnO are combined by Yu et al., [7] in which nanosheet networks on hexagonal pyramid like microcrystals are studied for their catalytic performance. In this complex structure, electrons are transferred from the NSs of high electric potential to the core micro pyramid of low electric potential which reduces the probability of photogenerated *e/h* recombination. NiO hollow microspheres showed significant catalytic activitythan rods [6] because the microspheres facilitate higher density of active sites and better surface charge carrier transfer rate.

Semiconducting niobate NSs were integrated [220, 221] into two component nanostructures system with separate sites for water reduction and oxidation. Although WO_3 is inactive for H_2 evolution its derivative $Na_2W_4O_{13}$ is active for overall water splitting from aqueous solution containing SRs where the later has layered structure (see Ref. 247 in [222]). Also see Bi_2WO_6 nanoplates in Ref. [206]. Kale et al., reported that $CdIn_2S_4$ nanostructures with a marigold-like morphology composed of numerous nanosized petals displayed significant H_2 production from H_2S in KOH aqueous solution [8].

A special class of 2D NSs are self-assembled into 3D architecture is another important research area of photocatalysis [6-11]. In the recent years, layered titanates were introduced for H_2 production due to their proton exchange capability in the absence of co-catalysts [223, 224]. Sodium trititanate ($Na_2Ti_{3-x}M_xO_7$), potassium tetratitanate ($K_2Ti_{4-x}M_xO_9$) and their substituted samples with SiO_2 pillared structures at the interlayer depicted higher activities [223], where M = Mn, Fe, Co, Ni, Cu and x varies 0.15-0.30. The effect of BET SA of the un-substituted tri and tetratitanates with respect to the H_2 generation is presented in Fig. 22. Layered double hydroxides have general formula of $[M^{II}_{(1-x)}M^{III}_x(OH)_2]A^{n-}_{x/n}\cdot mH_2O$, where M^{II} is divalent metal cation (Mg^{2+}, Co^{2+}, Ni^{2+}, Zn^{2+}, etc) M^{III} is trivalent metal cations (Al^{3+}, Cr^{3+}, Ga^{3+}, Fe^{3+} etc) and A^{n-} can be organic and/or inorganic anions (see references 2-4 in Ref. [209]). The specialty of these layered hydroxides lies in the fact that they can be doped with a cation at the octahedral sites which yields their properties similar to doped semiconductors. Fe^{3+} incorporated Mg/Al layered double hydroxide depicted significant H_2 production [209]. Compton et al., [220, 221] reported calcium niobate ($HCa_2Nb_3O_{10}$) NSs with Pt for the photochemical H_2 generation. Ferroelectric materials such as stibiotantalites, $SbMO_4$ (M = Nb, Ta) were investigated for H_2 production in the form of NPs [208]. The H_2 evolution rate of $SbTaO_4$ (3.72 eV) is approximately 2 times higher than that of $SbNbO_4$ (3.12 eV) which is further enhanced after RuO_2 co-catalyst incorporation. The differences in the activity are attributed to the higher CB edge of $SbTaO_4$ (Ta 5d orbitals in TaO_6 octahedra configuration) and high dielectric constant where the latter enhances the photogenerated charge separation.

Polyoxometalates such as $Bi_2W_2O_9$, $BaBi_4Ti_4O_{15}$, Bi_3TiNbO_9 etc layered structures are highlighted for H_2 evolution in a review article by Yamase [225] in the presence of SRs. On the other hand scheelite structured $PbMoO_4$ shows activities for H_2 and O_2 evolution in the presence of SRs under UV irradiation. The substituted compounds $Na_{0.5}Bi_{0.5}MoO_4$, $Ag_{0.5}Bi_{0.5}MoO_4$, $Na_{0.5}Bi_{0.5}WO_4$ and $Ag_{0.5}Bi_{0.5}WO_4$ are also active for O_2 evolution [222]. Although molybdates and tungstates respond only to UV, Pb, Bi and Ag play an important role in the structure of VB. Solid solutions of b-Ga_2O_3 and In_2O_3 consisting of d^{10} cations have been systematically studied for H_2 or O_2 evolution from aqueous solutions in the presence of SRs. In these catalysts the band gap and luminescent energy decrease as the ratio of indium increases [222].

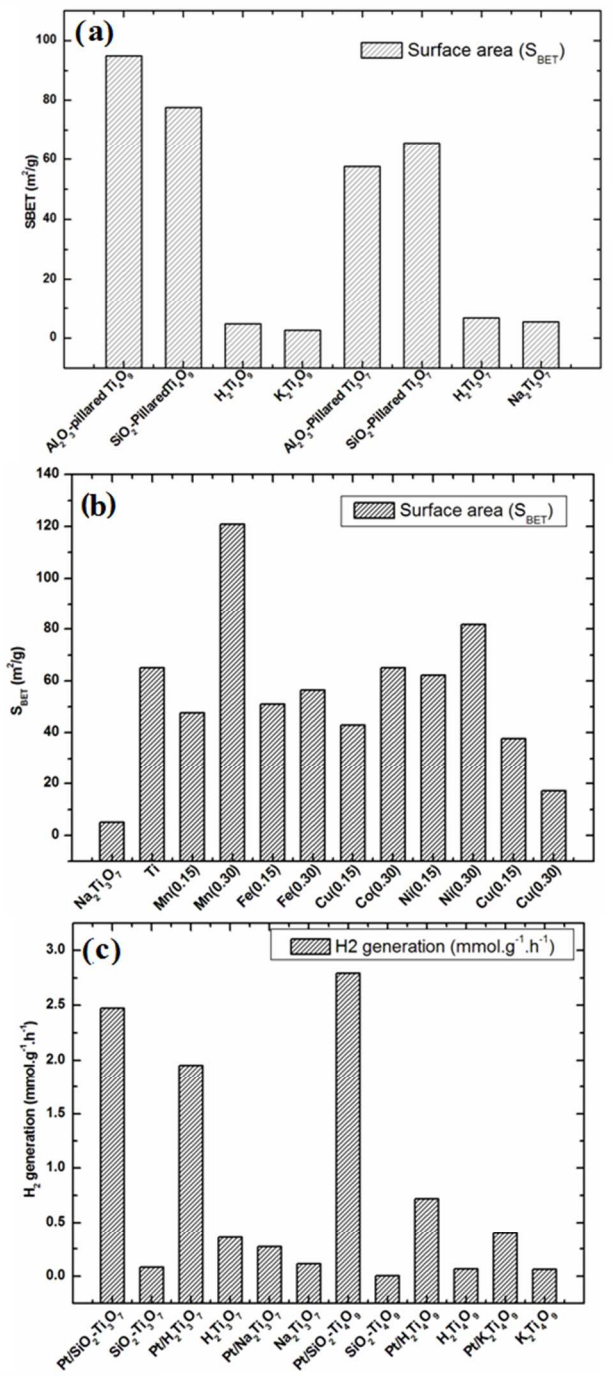

Figure 22: Properties of different semiconductors (a), (b) surface area and (c) H_2 production [223].

Sabio et al., [226] reported that the hydroxide supported calcium niobium ($HCa_2Nb_3O_{10}$) NSs presented superior H_2 production rate under UV irradiation in the presence of SR or co-catalysts. NSs produced at high rate of H_2 compared to their bulk counter parts. As the structural conversions of TiO_2 NPs to NSs also proved their high catalytic activity for H_2 generation and removal of environmental pollution [227]. Pt-loaded TiO_2 hierarchical photonic crystals [41] have shown double efficiency. The rate of hydrogen production is 247 μmol.h^{-1} and the QY is ~11.9 %. The experimental results show that stop band reflectivity was suppressed and slow photon enhancement dominated enhancing the H_2 evolution. Zhou et.al[81] constructed a leaf like structure by copying the complex architecture of leaf by replacing the natural photosynthetic pigments with man-made catalysts and realized an efficient catalyst.. Since the utilization of 20% of aqueous methanol as SR might have improved the H_2 evolution rate.

Table 2: UV active nanocatalysts for water splitting.

Catalyst	SA (m^2/g)	E_g (eV)	Co-catalyst/ SRs	Light source UV-Vis	Catalytic activity H_2	Ref

					μmol/h	
Nanowires						
$LiNbO_3$	28		RuO_2	300-W Xe	275	[26]
$LiNbO_3$	28		RuO_2	400-W Hg	47	[26]
Si/Cu_2O			Pt/Na_2SO_3-Na_2S	300 W Xe	95	[59]
$ZnO/Zn_xCd_{1-x}Te$		1.48	Na_2SO_3-Na_2S	300 W Xe	265	[35]
CdSe/CdS N-doped TiO_2			Pt	520 nm LED	434.29	[126]
N-doped TiO_2			Pt/ EtOH-H_2O	3.15 W UV-A	700	[127]
				3.0 W UV-B	2250	[127]
Nanotubes						
TiO_2			Pt/Ag	365 nm, 50 mW/cm2	10.69	[139]
TiO_2			Pt/ EG (NH_4F-H_2O)	300 W Xe	420	[146]
Ti−Fe−O			Pt/KOH	300 W Xe	7.1mL/W,h	[128]
Titania			Pt	50 W metal hydride	960 μmol/h W	[129]
NiO_x-$SrNb_2O_6$	8.1		Pt	450 W Hg	102	[46]
TiO_2			Pt/EtOH-H_2O	150 W X*e/h*g	0.98	[144]
TiO_2			Pt/glycol and NH_4F	300 W Xe	0.57 ml/h cm2	[145]
W-TiO_2			Na_2S+Na_2SO_3	300 W Xe	24.97	[147]
Ta_2O_5	16.2		EtOH-H_2O	240 W Hg−Xe	2600	[148]
TiO_2			NH_4F/ethylene glycol (ETG)/Au	150 W Hg-Xe	0.65 μmol/cm^2/h	[136]
CNT	194		Eosin-Y (EY)- TEOA	Solar simulator (100 mW/cm^2)	18	[68]
Pd/ TiO_2			Na_2CO_3 and EG	300 W Xe	592 μmol·h $^{-1}$.cm^{-2}	[140]
Nanorods						
$SrSnO_3$	0.5	4.1	$Pt/AgNO_3$	200 W Hg-Xe	8200	[154]
$(Cd_{0.8}Zn_{0.2})S$	72	2.4	SO_3^{2-} (Na_2SO_3)	300 W Xe	1710	[143]
			S^{2-} (Ns_2S)	300 W Xe	3020	[143]
Zn_2GeO_4			MeOH	125 W Hg	6240	[77]
	33.2	4.67	Na_2SO_4	125 W Hg	6000	[76]
			MeOH	150 W Hg	430	[157]
	36	4.67	MeOH-H_2O	300 W Xe	4900	**[158]**
	33.1		RuO_2	300W Xe	17.4	[25]
In_2O_3–In_2S_3			MeOH-H_2O	300 W Xe	61.4	[159]
TiO_2	64.19		MeOH-H_2O/Cu^{2+}	400 W Hg	3000	[152]
Nanofibers						
TiO_2	56.3		MeOH	450-W Hg	54	[117]
SrTiO3	31.3		MeOH	450 W Hg	167	[120]
SrTiO3/TiO_2	98.26		MeOH-H_2O	400 W Hg	~1100	[198]
Au/Pt/TiO_2		3.2	L-ascorbic acid	300 W Xe	11.66	[118]
TiO_2/SrTiO3	98.26		MeOH-H_2O	400 W Hg	1100	[121]
TiO_2	47.45			400-W Hg (UV)	90	[121]
TiO_2 (500 °C)	96.3			visible	206	[85]
TiO2 (500 °C)	58.2			450 W Hg	19.1	[93]
TiO_2/Pt (500 °C)	96.3			>420 nm (visible)	7110	[85]

TiO_2/CuO (450 °C)	108.1			400-W Hg (UV)	62.7	[228]
TiO_2/SnO_2 (450 °C)	73.1		MeOH-H_2O	400-W Hg (UV)	200	[119]
TiO_2/MWCNT	600		Pt/parylene	150 W Xe	691	[44]
Nanolayers						
$SbNbO_4$	1.66	4.1	RuO_2	450 W Hg	24	[208]
$SbTaO_4$	1.53	3.9	RuO_2	450 W Hg	58	[208]
Fe^{3+}-Mg/Al	62		MeOH	125 W Hg	301	[209]
Nanoribbons						
CdSe			Na_2SO_3-Na_2S	175 W Hg	106.79	[115]
Nanoleaf						
$Na_2Ti_4O_9$		4.11	MeOH-H_2O	350 W Hg	5.72	[211]
Nanosheets						
Pt/TiO_2	94		EtOH	350-W Xe	333.5	[217]
Nanosheets						
$HCa_2Nb_3O_{10}$		3.53	Pt	175 W Hg	78.37μmol	[220]
$HCa_2Nb_3O_{10}$		3.53	Pt	175 W Hg	49.15	[221]
Tetrabutyl ammonium-$Ca_2Nb_3O_{10}$			Pt/MeOH-$AgNO_3$	350-W Xe	3231.40	[226]
TiO_2			MeOH-H_2O	150 W Xe	6000	[227]
Flower TiO_2 (500 °C) Anatase	31.7		MeOH-H_2O	450 W Hg	117.6	[219]
FL TiO_2 (500 °C)	31.7			450 W Hg	588	
Photonic Crystals						
TiO_2	75.5		CH_3OH	500 W Xe lamp	247 μmol.h^{-1}	[41]
N-TiO_2leaf	103.31		Pt/ Methanol	400 mW/cm^2 Xe lamp	1401.70 μmol.h^{-1}	[81]

5. Modified visible light active photocatalysts for hydrogen generation

As mentioned earlier, photogenerated electrons easily recombine with holes in semiconductor. This recombination leads to the low quantum efficiency (QE) of photocatalysis. It has been reported that the SRs can effectively restrain this recombination process and improve QE. Several common approaches have been adopted to activate the wide band gap materials to the visible light for water splitting *viz* (1) doping metal or/and nonmetal ions, (2) controlling the band structure via developing solid solutions, (3) dye sensitization, (4) band gap engineering, (5) combining wide band gap materials with visible active semiconductors etc. The visible light activity of the nanostructured materials has been important in enhancing the efficiency of electron injection to the CB of a photocatyst. The following subsections provide full details of different nanostructures and their modifications to obtain visible light activity.

5.1. Nanowires

Fabrication of variety of nanostructures and doping therein has improved the activity of PEC water splitting. Confined dimensionality 1D and 2D offers an enhanced light absorption due to large active SA and ultrafast charge transport behavior. In the introduction of this article we have outlined the thermodynamic requirement [24] which is unavoidable for any catalyst not to corrode. However CdS (E_g = 2.4 eV) is very effective in the visible light water splitting [229] in the presence of SRs such as S^{2-}, SO_3^{2-} etc. The effect of SA and H_2 generation with respect to the synthesis-temperature is shown in the Fig. 23. It can be seen that as the synthesis temperature increases the H_2 evolution also increases despite of fall in the SA (Fig. 23a). Furthermore, the rate of H_2 production was improved by incorporating graphitic (gC_3N_4) structures with CdS under visible light irradiation, see Table 3 and Ref. [231]. In the presence of Pt and SRs, CdS has shown further improvement in H_2 production [104]. Titanic acid NWs/EY in the presence of Pt NPs and TEOA has shown to yield significant H_2 [232]. The performance of NWs was significantly improved by introducing Au NPs [137], where it is also noted that the yield depends on the shape and structure of Au. Kibria et. al., [233] reported GaN NW photocatalysts for spontaneous water splitting to produce H_2 under visible and infrared light irradiation.

Moving on to the heterostructures, CdS/TiO_2 NTs were investigated for H_2 production [234] and the results suggests a QE of ~43.4% under visible light (~420 nm). The high activity is because of the quantum size effect and the potential gradient at the interface [234]. Liu et al., [235] combined Si (cathode) and TiO_2 NWs (anode) where the difference in the band gap of these materials as well as band alignment are notable (Fig. 24a). See the SEM pictures in Fig. 24b and c. In this case under illumination *e/h* pairs are generated in Si and TiO_2 while absorbing different wavelength regions of the solar spectrum. See the band bending in Fig. 24d which favors the transfer of electrons from TiO_2 to recombine with holes in Si. The electrons from Si and holes from TiO_2 take part in H_2 and O_2 generation

respectively.

1D NWs of multi band gap metal nitride (InGaN/GaN) heterostructure facilitates efficient matching and utilization of incident solar irradiation [236]. In this recent study [236] InGaN/GaN NWs with various doping levels of In facilitated broad absorption wavelength range with co-catalyst, Rh-Cr_2O_3 core-shell NPs [237]. Figure 25a shows the SEM image of GaN/InGaN NWs grown on GaN nanowire templates on Si(111) substrate while Fig. 25b suggests the reaction mechanism on the co-catalyst and InGaN/GaN NWs. Water splitting takes place on both GaN and InGaN nanowire (Fig. 25c) under suitable illumination. As expected with the increasing wavelength apparent QE decreases (Fig. 25d). Similar work with GaN and InGaN heterostructures can be seen from the same research group [238].

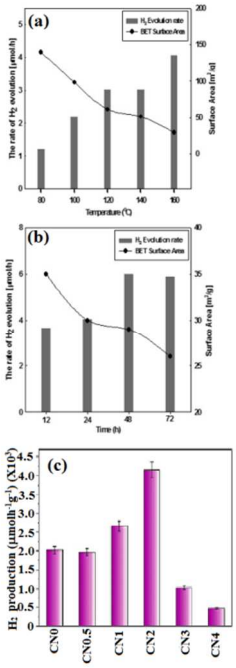

Figure 23: (a) Rate of H_2 evolution and the surface area of CdS samples synthesized by solvothermal reaction at different temperatures, (b) synthesis at 160 °C for 12 h, 24 h, 48 h and 72 h. Catalysis: 0.1 g CdS with 1 wt% Pt, 0.1 M Na_2S+0.02 M Na_2SO_3, 500 W Hg-lamp with a cutoff filter ($\lambda \geq 420$ nm) [229] and (c) H_2-production from CdS nanowires (CN0) and g-C_3N_4-coated CdS nanowires (CN0.5, CN1, CN2, CN3 and CN4) from 0.35 M Na_2S+0.25 M Na_2SO_3 aqueous solution[231].

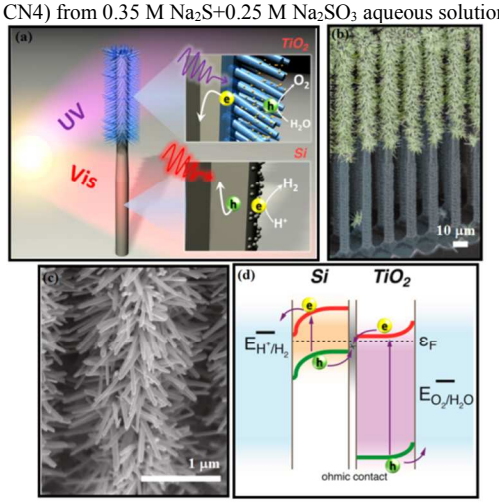

Figure 24: (a) Schematic diagram of Si/TiO_2 tree-like heterostructures, (b) false-colored SEM image of a Si/TiO_2 nanotree (c) magnified SEM image and (d) band diagram of the two components[235].

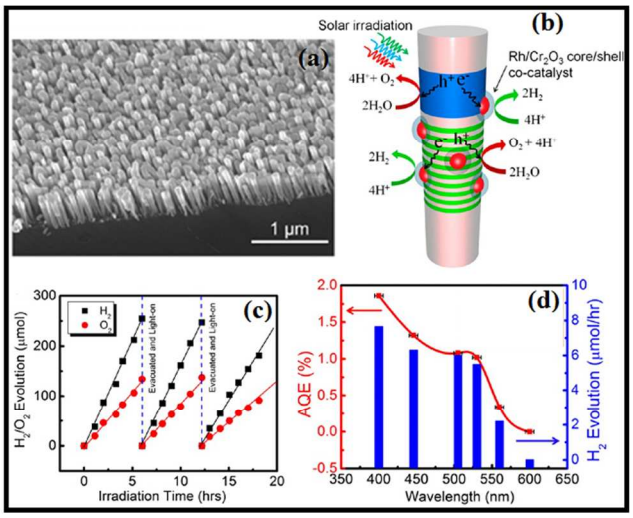

Figure 25: (a) SEM image of GaN/InGaN nanowire grown on Si substrate, (b) water splitting mechanism on Rh/Cr_2O_3/InGaN/GaN, (c) irradiation time versus H_2/O_2 evolution and (d) apparent quantum efficiency (AQE) and H_2 evolution rate against incident wavelength (full-width-half-maximum of the optical filters is given as error bars. The H_2 evolution rate was derived from ~2 h of overall water splitting under each optical filter[236].

5.2. Nanotubes

In general surface defects such as oxygen vacancies on the semiconductors play a crucial role in catalysis. [36, 172, 173, 239-242] The oxygen vacancies serve as adsorption sites as well as help to delay the recombination in semiconductor [36, 172, 173] depending on their physical location within the catalyst. In the case of TiO_2 NT, Kang et al., [243] suggested $NaBH_4$ treatment to control the defects on the surface. The treated surface has better electron transfer properties at the semiconductor/electrolyte interface than the parent surface.

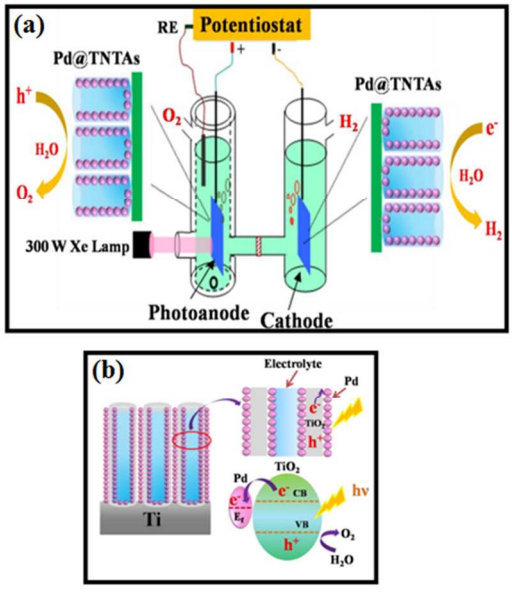

Figure 26: (a) Schematic of a PEC cell with Pd-TiO_2 NTs and Pt-TiO_2 NTs. Close-ups show both photoanode and cathode and (b) schematic diagram of Pd QDs-TiO_2 NTs and the charge transfer process from TiO_2 to Pd (lower right panel) [140].

However, predominant oxygen vacancies will not help to enhance the H_2 production. Similar results are obtained on surface fluorinated-TiO_2 nanoporous films. TiO_2 NTs with Pd QDs as co-catalyst facilitated relatively higher efficiency photocatalytic H_2 generation [140] see Fig. 26a for the schematic of PEC cell and Fig. 26b for electron transfer and H_2 production.

1D nanostructured titanate NTs are known for their cation-exchange capacity which allows high loading of active catalysts as shown by Li et al., [245] where $Na_2Ti_2O_4(OH)_2$ NTs were investigated in the presence of Triethanolamine (TEA) and Pt. Interestingly, titanates are investigated for their photocatalytic degradation of dye molecules [171] while they need to be considered for H_2 production too because of the predominant surface defect densities which help to enhance the catalysis.

Li et al., [246] reported that EY/MWCNTs in the presence of TEOA (electron donor) have shown significant H_2 generation under visible light illumination ($\lambda \geq 420$ nm). The role of MWCNT is similar to the noble metals in the context of delaying the recombination by trapping the electrons and can be a good substitute for Pt. Earlier seen type I and type-II band alignments consists of two semiconductors such as CdS/TiO_2 [244] while ternary (CdS/TiO_2/Pt and CdS/TiO_2/CNTs) and quaternary composites (CdS/TiO_2/Pt/CNTs) also demonstrated significant H_2 generation. In all of these cases the cascaded charge transfer takes place between TiO_2 and CdS while Pt and/or CNTs act as electron collecting materials [247]. In Ref. [244] TiO_2 is in the form of NTs which are modified with CdS nanostructures as shown in Fig. 27a. *p*-type Cu−Ti−O NTs with *n*-type TiO_2 NTs have shown significant the photocurrent generation while it is self biased due to suitable band alignment, see Fig. 27b [132]. CdS-trititanate NTs have been investigated for their H_2 generation capability and the results suggest that the effective charge separation is evidenced in this composite which favors the catalytic activity [248].

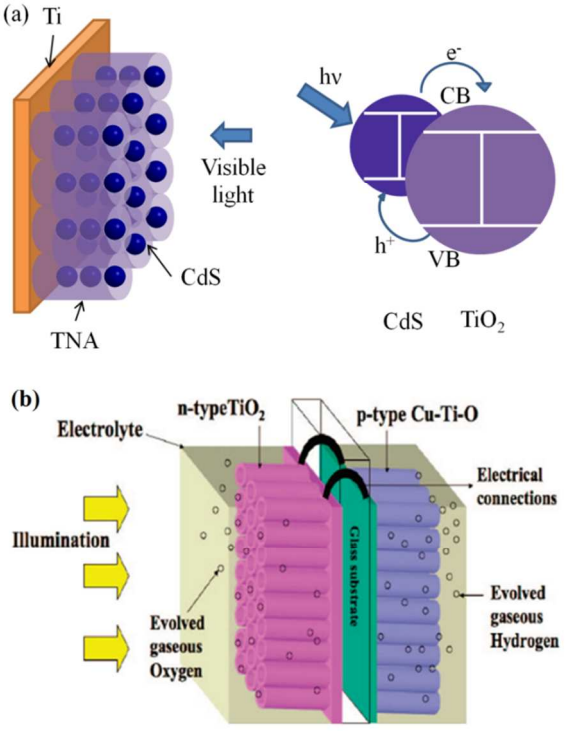

Figure 27: (a) Schematic diagram of CdS-TiO_2 NTs (left) and the charge transfer process (right)[244], (b) PEC diode consisting of TiO_2 and Cu-Ti-O NT arrays. The oxygen evolving TiO_2 side absorbs UV and Cu-Ti-O side absorbs the visible part of the spectrum evolving H_2 [132].

5.3. Nanorods

Incorporation of small amount (~1%) of copper ions into TiO_2 NRs have shown improved performance than their pure counterparts under solar light [249]. The doping has caused the band gap to shrink from 3.10 eV to 2.84 eV. However, further decrease in the E_g (2.40 eV at ~3% Cu doping) has decreased the H_2 production by ~5 times in pure water.

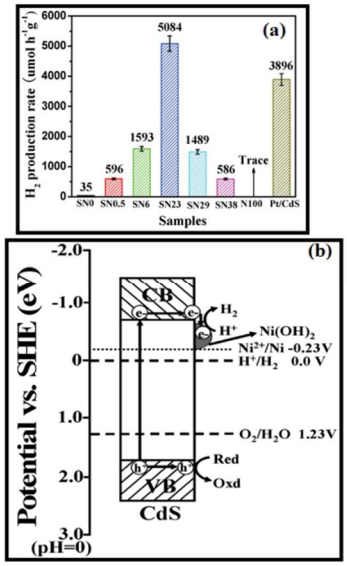

Figure 28: Comparison of H_2-production for various ratios of CdS to $Ni(OH)_2$ (SN). The ratios are given in brackets for various samples SN0

(0), SN (0.5), SN (6), SN (23), SN (29), SN(38), N (100) samples and 1 wt% Pt-CdS under visible light with TEA aqueous solution and (b) proposed mechanism for H_2 production [250].

Interestingly, in the presence of MeOH aqueous solution the H_2 production from 1% and 3% Cu doped TiO_2 are comparable. This study suggests that having lower band gap may not help to enhance the photon harvest in all cases. Severe doping might cause lattice defects or secondary phase formation which might act as electron traps thereby decreasing the H_2 production. However, if the density of hole traps can be increased then H_2 productivity can be increased or at least back reactions can be minimized. The morphology and crystal quality helps to enhance the H_2 generation as seen in the case of CdS NRs and nanograins, where the former has shown better results [113]. CdS NRs modified with $Ni(OH)_2$ (23 mol%) exhibited highest H_2 generation under visible light irradiation [250] (see Fig. 28a and its legend for various levels of modification). From Fig. 28b we can see that the potential of Ni^{2+}/Ni is lower than the CB of CdS and more negative than the H^+/H_2 potential. This alignment favours the electron transfer from CB of CdS to $Ni(OH)_2$ and the reduction of H^+ into H_2. By given the band gap of iron oxide (corresponding to visible range absorption), maghemite (γ-Fe_2O_3)-hematite (α-Fe_2O_3) core-shell NRs were produced and they have shown higher H_2 evolution with reference to their individual NRs [251] from H_2S. Porous $ZnFe_2O_4$ NRs showed effective H_2 evolution from aqueous methanol solution under visible light where the shapes and intraparticle porous structure are beneficial for quick transfer of photogenerated carriers onto the surface [252]. Interestingly, O_2 evolution is not detected in this context which can be because of mismatched energy levels of VB (of $ZnFe_2O_4$) and the oxidation potential of water. Surprisingly, without using any SRs Au NRs/TiO_2 cap/Pt NPs configuration [253] produced H_2 of ~2.8 mmol $h^{-1}g^{-1}$. The improved H_2 evolution was because of the promotion of trap bound electrons in the TiO_2 to its CB. These electrons were then captured by Pt to participate in the H_2 evolution (see the Ref.[150]).

5.4. Electrospun Nanofibers

Metal oxide composite nanofibers [228, 254] also proved to be efficient in H_2 generation. Zhang et.al., [255] reported plasmon enhancement on photocatalytic H_2 generation over Au/Pt/TiO_2 electrospun nanofibers.

Yousef et al., [256] suggested that the incorporation of the transition metal NPs can strongly modify the physiochemical characteristics of the metal oxides nanostructures. Lee et al., [254] have shown that TiO_2/CuO composite NFs can be promising for H_2 production. Typical SEM image of the electrospun fibers and H_2 production over time were given in Fig. 29a to c. The charge generation and subsequent catalysis is given in Fig. 29d. Almost similar work by the same research group has been published elsewhere too[228]. It has been reported that the combination of Fe_2O_3 nanoparticles TiO_2 NFs has drawn advantages from both the materials and enhances the light absorption[257]. As an effective strategy to overcome the photocorrosion and toxicity problems from CdS based materials is to incorporate them in polymeric nanofibers. Such as the case with CdS and CdS-PdS NPs. They were mixed in poly(vinyl acetate) electrospun nanofibers and the composite produced more H_2 than bare CdS NPs [258]. Apart from the earlier discussed reasons, the efficiency of H_2 generation depends on the morphology of NFs [83]. Yang et.al [83] reported that the electrospun core-shell (CdS-ZnO) NFs exhibited excellent H_2 generation under visible light where the activity is mainly attributed to high visible light absorption and low charge carrier recombination. Nitrogen doped-TiO_2 electrospun nanofibers were also explored for efficient H_2 generation where the efficiency is found to be dependent on the concentration of the nitrogen precursor content [45]. Caterpillar-like ZnO nanostructures on ZnO forcespun nanofibers shown ~0.165% of photon-to-hydrogen conversion efficiency[259] where the increase is accounted to the enhanced light harvesting ability and the effective electron hole separation.

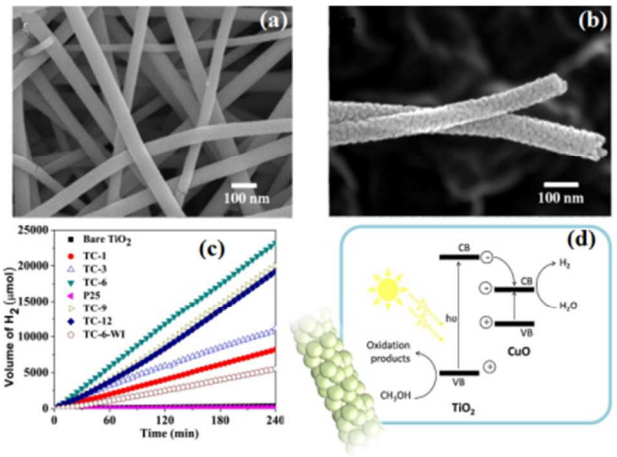

Figure 29: (a) FE-SEM images of TiO_2-CuO at 6 mol% of Cu NFs (b) high magnification FE-SEM image, (c) H_2 evolution and (d) schematic band diagram of TiO_2/CuO heterojunction [254].

5.5. Two dimensional nanostructures

5.5.1. Nanosheets

The CdS NSs produced by two step synthesis were able to produce H_2 of ~4.1 mM/h under visible light [260] (Fig. 30a). From the previous results it is evidenced that Pt is an excellent co-catalyst. However, it is vital to quantify its loading percentage. As expected excessive loadings may not help to increase the yield (Fig. 30b). The optimum value can be seen from Fig. 30b. This study also optimizes the concentration of SRs and H_2 evolution from various cycles, see Fig. 30c and d. ZnS by given its band gap (E_g=3.4 eV) is not active in the visible region in contrast $ZnIn_2S_4$ [261] where the latter has shown nearly 5 times higher activity in the presence of Pt than its pristine counterpart in the visible region. ZnS is studied in combination with CuS/Cu_2S in the form of NSs in the presence of Na_2S and Na_2SO_3 [88]. The H_2 production rates from different catalyst combinations can be seen from Fig. 31a. Pristine ZnS (CZ0) shows a negligible amount of H_2 production, since the band gap of ZnS is too large to absorb visible light. In contrast after addition small amounts of CuS to ZnS the H_2 generation is abruptly increased under visible light exposure. The H_2 production mechanism for the CuS/ZnS porous NSs is shown in Fig. 31b.

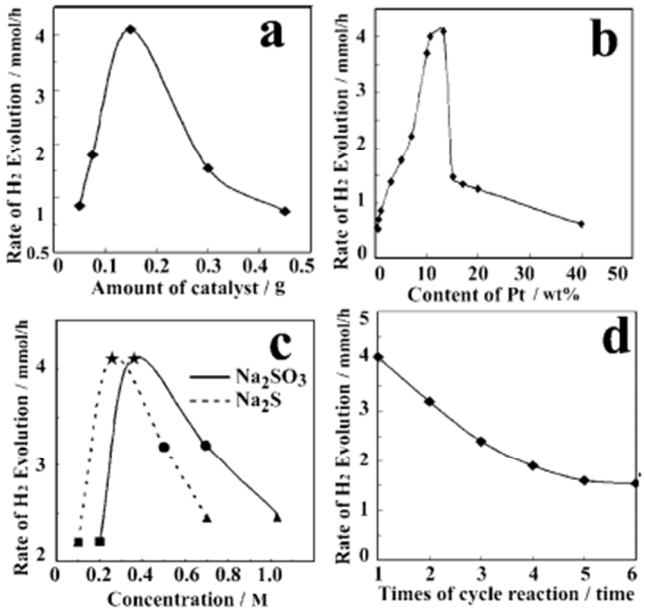

Figure 30: H_2 evolution (a) quantity of CdS catalyst with 10 wt % Pt, (b) Pt-loading (0.15 g of CdS), (c) concentration of SRs against H_2 evolution rate from 0.15 g of Pt-CdS and (d) 0.15 g of 10 wt % Pt-CdS. (a) (b) and (d) uses 0.25 M Na_2SO_3+0.35 M Na_2S electrolyte. All reactions were performed under visible-light [260].

Obviously the band-to-band transition of ZnS cannot take place under visible light irradiation due to the large band gap energy. Pure CuS also shows no visible light activity while interestingly the combination of CuS/ZnS provide a platform for the visible activity. In Ref. [88] the authors did not mention about the VB of CuS/Cu_2S, however, the band diagram suggests a band gap of 2.94 eV where the VB of ZnS and CuS/Cu_2S are at the same energy level. If we consider the band diagram of CuS and Cu_2S from the literature, it appears to be the case that the VB of ZnS and CuS or Cu_2S are not energetically in line with each other (see Fig. 31c). If the interfacial charge transfer (IFCT) has to take place the energy difference from VB of ZnS to Cu_2S/CuS should be taken into account. Furthermore, by given the band gap range of 1.2 eV to 2.15 eV (CuS/Cu_2S combined) the 420 nm illumination is good enough to create *e/h* pairs in these semiconductors. In this case, the transfer of charge takes place from CuS/Cu_2S to ZnS.

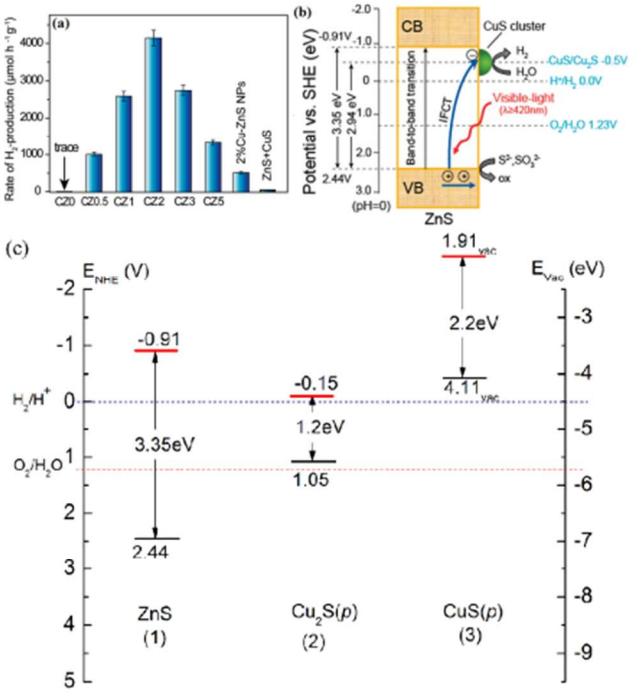

Figure 31: Comparison of H_2-production of CuS/ZnS porous NSs and ZnS samples under visible light in the presence of 0.35 M Na_2S+0.25 M Na_2SO_3, (b) schematic of interfacial charge transfer (IFCT) from the VB of ZnS to the CuS clusters [88]. CZ0-ZnS, CuS molar concentration is denoted as numerals. (c) energetic values of the CB and VB positions of ZnS, Cu_2S and CuS are taken from the corresponding references as follows. ZnS (1) [88], Cu_2S (2) [262, 263] and CuS(*p*) (3)[264].

Moreover, interfacial regions are generally defective and hence we can expect charge carrier traps within the interface. Another combination of heterostructure is NiO-CdS[265], where CdS absorbs the visible light and photogenerated electrons are transferred to NiO. This combination has shown significant H_2 production as shown in Fig. 32a. While Fig. 32b depicts the band alignment and corresponding charge transfer phenomenon under visible light irradiation.

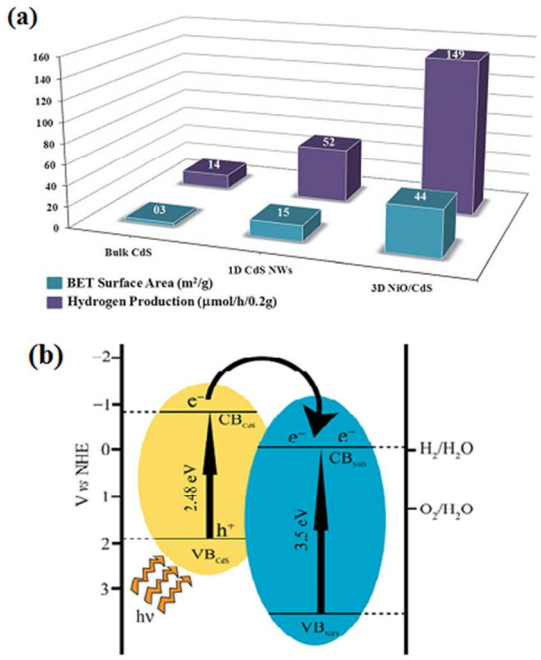

Figure 32: (a) Surface area and the amount of H_2 generation from CdS bulk, 1D CdS NWs and 3D NiO–CdS photocatalysts under visible light irradiation and (b) Schematic illustration of electron transfer and the band diagram of NiO and CdS [265].

In the context of graphene, apart from its outstanding electrical conductivity, it can inhibit the recombination of the electron hole pairs by collection the electrons and enhance the visible light absorption. This phenomenon is similar to that of noble metal NPs [266]. The mechanism and the influence of the graphene oxide with CdS clusters for the high efficiency visible light driven photocatalytic H_2 production is shown in Fig. 33 [266].

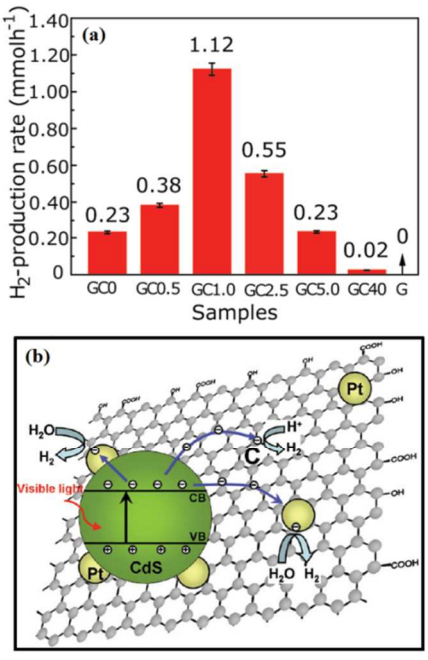

Figure 33: (a) Graphene oxide CdS composite and H_2 productivity in the presence of 10 vol % lactic acid aqueous solution and 0.5 wt % Pt and (b) charge generation and subsequent separation under visible light [266]. The weight ratios of GO to $Cd(Ac)_2$ $2H_2O$ were 0, 0.5%,1.0%, 2.5%, 5.0%, and 40%, and the obtained samples were labeled as GC0, GC0.5, GC1.0, GC2.5, GC5.0, and GC40, respectively.

5.5.2. Nanolayers

Simulation studies [267] on MoS_2 layered structure suggest that the pristine single-layer MoS_2 is a good candidate for H_2 production. The catalytic activity can be improved by applying a small in-plane compressive strain or out-of-plane tensile strain. On the other hand, *p*-type doping (with phosphorus) can also be employed to enhance the overall water splitting. The changes those occur due to the doping are schematized in Fig. 34. Layered Zn-In-S photocatalyst in the presence of NaCl has also shown high visible-light activity for H_2 evolution[268]. Morphologically similar structures are produced with $ZnIn_2S_4$ and tested their activity for H_2 production [269].

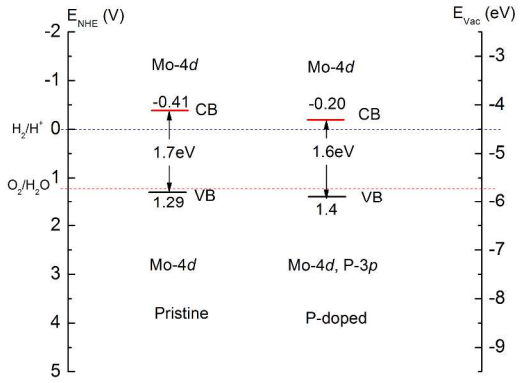

Figure 34: The band diagram of single layer MoS_2 and its P-doped counterpart. Figure redrawn based on Ref.[267].

5.5.3. Nanoribbons

Earlier we have seen that MoS_2 layered structure can be potential for H_2 evolution. In this instance, MoS_2 layers are exfoliated via ultrasonication and chemically linked to CdSe nanoribbons. The resultant composite has shown a QY of 9.2% at 440 nm, whereas bulk CdSe is not active for the reaction. The overall increase is nearly four times which of course depends on the mass percentage of MoS_2. It is interesting to see that chemical linkage of Pt NPs to the CdSe nanoribbons did not influence the H_2 evolution [270].

5.5.4. Metal-free photocatalyst

Graphitic carbon nitride (g-C_3N_4) is a potential material for H_2 production from water under visible light illumination [271]. Under suitable illumination creation of *e/h* pairs is similar to metal oxide photocatalysts, where electrons are excited to CB and holes are created in the VB. In the present example, oxidation of H_2O takes place at nitrogen atoms, while the carbon atoms provide the reduction sites for H_2, see Fig. 35. Similar study can be seen in the literature [271].

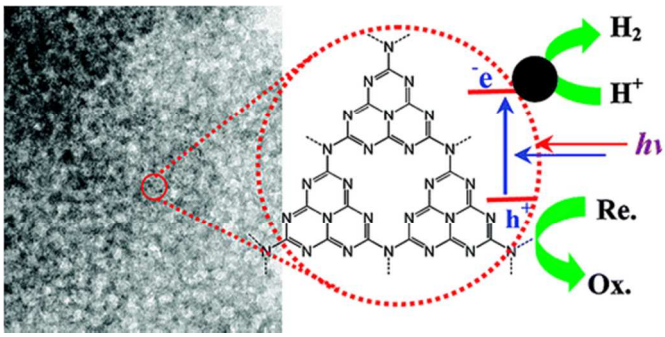

Figure 35: TEM image of g-C_3N_4 and H_2 evolution under visible light illumination. Figure reproduced with permission from Ref. [272].

The 1D graphitic carbon nitride NRs were template synthesized and decorated with Pt NPs [273]. This hybrid material demonstrated surprisingly high H_2 yield with low specific SA in the presence of triethanolamine scavenger. The enhancement is ascribed to the efficient charge separation of the 2D layered structures. Huang et.al[274] reported bio-inspired carbon nitride mesoporous NSs composed of nanospheres and demonstrated H_2 generation possibility.

Table 3: Visible active and/or modified nanocatalysts for water splitting.

Catalyst	SA	E_g	Co-catalyst/ SR	Light source	H_2 µmol/h	Ref
Nanowires						
CdS	29		Na_2S-Na_2SO_3	500 W Hg	4	229
CdS/g-C_3N_4	22.9		Na_2S-Na_2SO_3	350 W Xe	4152	231
C_3N_4			Pt			271
CdS	73.6	2.43	Na_2S-Na_2SO_3	300 W Xe	260	104
Titanic acid			Eosin Y-sensitized Pt/TEOA	300-W halogen	88.1	232
Rh/Cr_2O_3: p- GaN:Mg		3.4	MeOH	300-W Xe	4000	233
Si-TiO_2			H_2SO_4	150 mW/cm^2 (1.5 suns)	875	235
Rh/Cr_2O_3 on InGaN/GaN			Pt	300 W Xe	683	236
InGaN/GaN				300 W Xe		238
Nanotubes						
$Na_2Ti_2O_4(OH)_2$	400		EY/Pt/TEA	300 W halogen	75.45	245
MWCNT			EY/MWCNT/Pt/TEOA	300 W halogen	3.06 mM	246
CdS/TiO_2/Pt/CNTs				100 mW/cm^2	70	247
CdS/TiO_2		2.36		350 W Xe	30.3	244
TiO_2	NT		Na_2CO_3-ethylene glycol	300 W Xe	592	140
CuO/Trititanate	87		EtOH	300 W Xe	98	248
Nanorods						
$ZnFe_2O_4$	51		Pt/MeOH	250 W Xe	237.87	252
CuO/Trititanate	70			150 W halogen	139.03	249
α-Fe_2O_3	61		NaOH	300 W Xe	60 mL/h	251
(γ-Fe_2O_3)-(α-Fe_2O_3)	66		NaOH	300 W Xe	75 mL/h	251
Ni(OH) $_2$/CdS	90		Pt/triethanolamine	300 W Xe	5084	250
Graphitic carbon nitride	52		Pt/ triethanolamine	LED lamp	~28 µmol.h^{-1}	273
Graphitic carbon nitride	230		triethanolamine	500 W Xe	2.45 %	274
Nanofibers						
Au/Pt/TiO_2			L-ascorbic acid	300 W Xe	0.108	255
Cu/TiO_2						275
NiO-TiO_2-Carbon						256

CdS-ZnO		2.34	Na_2S-Na_2SO_3	500W Xe	~354	83
TiO_2/N_2 (450°C)	70			150-W Xe	28	45
Nanolayers						
Zn-In-S	44.2		Pt	400 W Hg	211.2	268
MoS_2						267
Nanoribbons						
CdSe-MoS_2			Na_2S-Na_2SO_3	300 W Xe	45	270
Nanosheets						
$ZnIn_2S_4$	165.4	2.43	cetylpyridinium bromide/ Na_2S/Na_2SO_3	250 W Hg	1544.8	269
$ZnIn_2S_4$	103	2.3	Na_2S/Na_2SO_3	300 W Xe >420 nm	57	261
			$Pt/Na_2S/Na_2SO_3$		257	
CdS/Graphene	48		Pt/lactic acid	350 W Xe	1.12 mL	266
CuS/ZnS	37.5		Na_2S-Na_2SO_3	350 W Xe	4147	88
CdS	112.8		Pt/Na_2SO_3	300 W Xe	4.1 mM/h	260
Flower						
NiO-CdS	44		Na_2S-Na_2SO_3	500 W halogen	149	265
Metal free						
mpg-$C_3N_{4/0.2}$	69		Pt/triethanolamine	500W Hg	149	272
g-C_3N_4	10		MeOH-H_2O	>420 nm	10.7	271
Microspheres						
$ZnIn_2S_4$ (prepared with 0.21g of CPBr)	165.4	2.43	Na_2S-Na_2SO_3	250 W Hg	766.8	269
$ZnIn_2S_4$ (prepared at pH 2)		2.34			1544.8	

6. Conclusions and future prospects

Nanomaterials have met with tremendous attraction and high expectations of generating innovations in many research areas for example in medicine, communication, materials development and energy and environment technology. At the same time there is growing concern that nanomaterials can also be hazardous to health and the environment. When it comes to energy sector nanomaterials can be potential as they can be used in energy absorbing materials, storage (such as batteries, fuel cells and solar cells)Although nanomaterials are seen to be the way of future requirement, still they have disadvantages. Since these particles are very small, problems can actually arise from the inhalation of such particles. Presently, nanotechnology is very expensive and further development can be costly. However, manufacturing difficulty can increase the cost of the product. In the realistic market the cost of the nanomaterials can be obtained from Ref. [276].

It is convincing that environmentally friendly and cost effective fuel is of great demand where H_2 production comes into picture. Although it is a promising technology it has considerable amount of challenges which require further development before it can be employed in industrial. One of the challenges is to fabricate a catalyst that harvests H_2 from a nonconventional energy resource such as solar energy with a significant efficiency. When it comes to the consideration of band gap of the semiconductor wide band gap materials cannot utilize the visible part of the solar spectrum. Some of the small band gap materials require SRs or otherwise unstable for long term usage because of the thermodynamic requirement of CB and VB positions. Albeit SRs can inhibit the back reaction by capturing photogenerated hole [93] they tend to form CO_2 instead of O_2 [124] which is of course an adverse effect for the environment. As an attractive point industrial waste (sulfides from aqueous solution containing S^{2-} and SO_3^{2-}) can be considered as SRs. Such methods not only clean the environment but also produce valuable H_2 energy. On the other hand wide band gap materials can be subjected to band gap engineering to enable their activity in the visible light via doping or creating intrinsic defects. Care should be taken with the intrinsic defects as they can act as electron traps reducing the production efficiency while hole traps are useful. In a broader sense defect mediated catalysis should be of prime importance. Interestingly, these two concepts require further attention as they are least investigated.

Delaying the recombination of photogenerated *e/h* pair is the primary objective to enhance the catalytic activity. The availability of these charge carriers on the surface of the catalyst is vital, especially the electrons. The transport of electrons to the surface can be improved by creating an internal electric field via forming heterojunctions. Vastly investigated heterojunctions are based on NW or NR which possess a crucial property of vectorial charge transport. Various methods have been employed to fabricate such one dimensional structures, however, electrospinning requires further attention because of its versatility in producing such structures.

Nevertheless, it is important to consider a semiconductor combination that drives electrons to the surface of the

heterocatalyst while in the background of various other combinations do separate *e/h* pairs. Furthermore, that combination should increase the solar energy harvest. For example, $Zn_xCd_{1-x}Te$ in conjunction with ZnO in heterostructure helps extends the absorption of solar energy into NIR region [35] and as a whole can be as high as ~22% of solar spectrum [35].

In the process of fabrication, inorganic nanostructures are generally subjected to thermal treatment(s); note the exceptions. Contextually various studies have shown the H_2 production dependency on the processing parameters such as calcination temperature, however, excessively high temperatures can decrease the output [93]. The calcination temperature is crucial to determine the quality of the crystal which in turn determines the H_2 evolution efficacy when balanced against the defect density. Note that the density of defect is process dependent as well. The catalytic activity is related to the number density of active sites which may not be directly related to the SA measured through N_2 adsorption and desorption curves. Irregularities on the surface might increase the SA however, not necessarily the increased area can be directly correlated to that of H_2 evolution. For example, although SA decreases H_2 evolution is seen to increase with synthesis temperature [229]. The characteristic defect density [239-242] may be obtained from photoluminescence in case if the catalyst depict. At a later stage, they can be correlated with the photocatalytic activity [36, 172, 173] which might give better understanding for the development of promising materials. To comment further on this, photoluminescence may be taken as a standard measurement to quantify the defect density from radiative recombinations. Interestingly SA and H_2 evolution are extensively studied in the literature, however a clear correlation is not obtained because of the fact that H_2 evolution depends on various other things such as catalyst properties [277], particle size [278], co-catalysts, SRs, sensitizers [85] and in particular the kinetics of the chemical reactions that lead to final O_2 and H_2 formation [279].

Finally, the following points needs to be considered for the design of efficient and cost effective photocatalyst. (i) band gap engineering for the improved photon absorption to overlap with solar spectrum as much as possible, (ii) increase the recombination time of the photogenerated excitons so that they can take part in photocatalysis and (iii) avoid back reaction to form water.

Acknowledgements

V.J.B. and S.V. thank The Scientific & Technological Research Council of Turkey (TUBITAK) (TUBITAK-BIDEB 2221, Fellowships for Visiting Scientists and Scientists on Sabbatical) for fellowship. T.U. thanks EU FP7-Marie Curie-IRG (NANOWEB, PIRG06-GA-2009-256428) and The Turkish Academy of Sciences– Outstanding Young Scientists Award Program (TUBA-GEBIP) for funding.

7. Notes and references

†-authors contributed equally

[a] *UNAM-National Nanotechnology Research Center, Bilkent University, Ankara-06800, Turkey.E-mail:vjbabu2002@gmail.com(vjbabu); svempati01@qub.ac.uk (SVempati)*
[b] *Institute of Materials Science & Nanotechnology, Bilkent University, Ankara, 06800, Turkey,E-mail:uyar@unam.bilkent.edu.tr (TUyar) Fax:+90(312) 290 4365;Tel: +90(312) 290 3571..*
[c] *NUS Center for Nanofibers and Nanotechnology (NUSCNN), NUS Nanoscience and nanotechnology Initiative (NUSNNI), National University of Singapore, Singapore-117576, E-mail:seeram@nus.edu.sg (SRamakrishna).*

1. Z. Zou, J. Ye, K. Sayama and H. Arakawa, *Nature*, 2001, 414, 625-627.
2. M. Ashokkumar, *Int. J. Hydrogen Energ.*, 1998, 23, 427-438.
3. H. Balat and E. Kirtay, *Int. J. Hydrogen Energ.*, 2010, 35, 7416-7426.
4. M. Ni, M. K. H. Leung, D. Y. C. Leung and K. Sumathy, *Renew. Sust. Energ. Rev.*, 2007.
5. K. Shimura and H. Yoshida, *Energy Environ.Sci*, 2011, 4, 2467-2481.
6. X. Song and L. Gao, *J.Phys.Chem.C*, 2008, 112, 15299–15305.
7. F. Lu, W. Cai and Y. Zhang, *Adv.Funct.Mater.*, 2008, 18, 1047-1056.
8. B. B. Kale, J.-O. Baeg, S. M. Lee, H. Chang, S.-J. Moon and C. W. Lee, *Adv.Funct.Mater.*, 2006, 16, 1349-1354.
9. W.-T. Yao, S.-H. Yu, S.-J. Liu, J.-P. Chen, X.-M. Liu and F.-Q. Li, *J.Phys.Chem.B*, 2006, 110, 11704-11710.
10. J. Zhang, F. Shi, J. Lin, D. Chen, J. Gao, Z. Huang, X. Ding and C. Tang, *Chem.Mater.*, 2008, 20, 2937-2941.
11. J. K. Zhou, L. Lv, J. Yu, H. L. Li, P.-Z. Guo, H. Sun and X. S. Zhao, *J.Phys.Chem.C*, 2008, 112, 5316-5321.
12. A. Fujishima and K. Honda, *Nature*, 1972, 238, 37-38.
13. A. J. Bard, *J. Photochem.*, 1979, 10, 59-75.
14. A. J. Bard, *Science*, 1980, 207, 139-144.
15. A. J. Bard, *J. Phys. Chem.*, 1982, 86, 172-177.
16. A. C. Ford, J. C. Ho, Y.-L. Chueh, Y.-C. Tseng, Z. Fan, J. Guo, J. Bokor and A. Javey, *Nano Lett.*, 2009, 9, 360-365.
17. A. B. F. Martinson, J. E. McGarrah, M. O. K. Parpia and J. T. Hupp, *Phys.Chem.Chem.Phys.*, 2006, 8, 4655-4659.
18. S. Hernandez, V. Cauda, A. Chiodoni, S. Dallorto, A. Sacco, D. Hidalgo, E. Celasco and C. F. Pirri, *ACS Appl.Mater.Interfaces*, 2014, 6, 12153−12167.
19. T. B. Singh, F. Meghdadi, S. Günes, N. Marjanovic, G. Horowitz, P. Lang, S. Bauer and N. S. Sariciftci, *Adv.Mater.*, 2005, 17, 2315–2320.
20. V. Chakrapani, J. Thangala and M. K. Sunkara, *Int.J.Hydrogen Eng.*, 2009, 34, 9050–9059.
21. K. Aryal, B. N. Pantha, J. Li, J. Y. Lin and H. X. Jiang, *Appl.Phys.Lett*, 2010, 96, 052110.
22. J. Hensel, G. Wang, Y. Li and J. Z. Zhang, *Nano Lett.*, 2010, 10, 478–483.
23. Z. G. Yu, C. E. Pryor, W. H. Lau, M. A. Berding and D. B. MacQueen, *J.Phys.Chem.B*, 2005, 109, 22913–22919.
24. A. Kudo and Y. Misekia, *Chem.Soc.Rev*, 2009, 38, 253-278.
25. S. Yan, L. Wan, Z. Li and Z. Zou, *Chem.Commun*, 2011, 47, 5632–5634.
26. K. Saito, K. Koga and A. Kudo, *Dalton Trans*, 2011, 40, 3909-3913.
27. D. Barreca, P. Fornasiero, A. Gasparotto, V. Gombac, C. Maccato, T. Montini and E. Tondello, *ChemSusChem.*, 2009, 2, 230-233.

28. W. Siripala, A. Ivanovskaya, T. F. Jaramillo, S.-H. Baeck and E. W. McFarland, *Solar Energy Mater Solar Cell*, 2003, 77, 229-237.
29. X. Zhao, P. Wang and B. Li, *Chem.Commun*, 2010, 46, 6768-6770
30. R. v. d. Krol, Y. Liang and J. Schoonman, *J.Mater.Chem*, 2008, 18, 2311–2320.
31. Y. Li and J. Z. Zhang, *Laser & Photonics Reviews*, 2010, 4, 517-528.
32. K. Shankar, J. I. Basham, N. K. Allam, O. K. Varghese, G. K. Mor, X. Feng, M. Paulose, J. A. Seabold, K.-S. Choi and C. A. Grimes, *J.Phys.Chem.C*, 2009, 113, 6327–6359.
33. M. Paulose, K. Shankar, S. Yoriya, H. E. Prakasam, O. K. Varghese, G. K. Mor, T. A. Latempa, A. Fitzgerald and C. A. Grimes, *J.Phys.Chem.B*, 2006, 110, 16179–16184.
34. Y. Izumi, T. Itoi, S. Peng, K. Oka and Y. Shibata, *J. Phys. Chem. C*, 2009, 113, 6706-6718.
35. X. Zhan, Q. Wang, F. Wang, Y. Wang, Z. Wang, J. Cao, M. Safdar and J. He, *ACS Appl.Mater.Interfaces*, 2014, 6, 2878-2883.
36. F. Kayaci, S. Vempati, C. Ozgit, I. Donmez, N. Biyikli and T. Uyar, *Nanoscale*, 2014, 6, 5735.
37. R. Sathre, C. D. Scown, W. R. MorrowIII, J. C. Stevens, I. D. Sharp, J. W. AgerIII, K. Walczak, F. A. Houleae and J. B. Greenblatt, *Energ. Environ. Sci.*, 2014, 7, 3264-3278.
38. T. Hisatomi, J. Kubota and K. Domen, *Chem.Soc.Rev*, 2014, DOI: 10.1039/c3cs60378d, Advance Article.
39. M. Zhou, X. W. D. Lou and Y. Xie, *Nano Today*, 2013, 8, 598-618.
40. G. Wang, Y. Ling, H. Wang, X. Lu and Y. Li, *J.Photochem.Photobiol.C.*, 2014, 19, 35-51.
41. J. Liu, G. Liu, M. Li, W. Shen, Z. Liu, J. Wang, J. Zhao, L. Jiang and Y. Song, *Energ. Environ. Sci.*, 2010, 3, 1503-0506.
42. E. C. Garnett and P. Yang, *J.Am.Chem.Soc.*, 2008, 130, 9224–9225.
43. L. Tsakalakos, J. Balch, J. Fronheiser, B. A. Korevaar, O. Sulima and J. Rand, *Appl.Phys.Lett*, 2007, 91, 233117.
44. J. B. Veluru, K. K. Manippady, M. Rajendiren, K. M. Mya, P. R. Rayavarapu, S. N. Appukuttan and R. Seeram, *Int.J.Hydrogen Eng.*, 2013, 38, 4324-4333.
45. V. J. Babu, M. K. Kumar, A. S. Nair, T. L. Kheng, S. I. Allakhverdiev and S. Ramakrishna, *Int. J. Hydrogen Energ.*, 2012, 37, 8897-8904.
46. I.-S. Cho, S. Lee, J. H. Noh, D. W. Kim, D. K. Lee, H. S. Jung, D.-W. Kim and K. S. Hong, *J.Mater.Chem.*, 2010, 20, 3979-3983
47. S. Ikeda, A. Tanaka, K. Shinohara, M. Hara, J. N. Kondo, K.-i. Maruya and K. Domen, *Microporous Mater.*, 1997, 9, 253-258.
48. M. C. Hidalgo, M. Aguilar, M. Maicu, J. A. Navío and G. Colón, *Catal.Today*, 2007, 129, 50-58.
49. A. Testino, I. R. Bellobono, V. Buscaglia, C. Canevali, M. D'Arienzo, S. Polizzi, R. Scotti and F. Morazzoni, *J.Am.Chem.Soc.*, 2007, 129, 3564–3575.
50. A. Datta, A. Priyam, S. N. Bhattacharyya, K. K. Mukherjea and A. Saha, *J.Colloid.Interface Sci*, 2008, 322, 128-135.
51. S. Y. Chae, M. K. Park, S. K. Lee, T. Y. Kim, S. K. Kim and W. I. Lee, *Chem.Mater.*, 2003, 15, 3326–3331.
52. G. Liu, C. Sun, H. G. Yang, S. C. Smith, L. Wang, G. Q. M. Lu and H.-M. Cheng, *Chem.Commun*, 2010, 46, 755-757
53. L. Zhang, J. Li, Z. Chen, Y. Tang and Y. Yu, *Appl. Catal. A Gen.*, 2006, 299, 292-297.
54. J. C. Yu, J. Yu, W. Ho and L. Zhang, *Chem.Commun.*, 2001, 1942-1943
55. T. Park, S. A. Haque, R. J. Potter, A. B. Holmes and J. R. Durrant, *Chem.Commun.*, 2003, 2878-2879
56. E. C. Garnett, M. L. Brongersma, Y. Cui and M. D. McGehee, *Annu. Rev. Mater. Res.*, 2011, 41, 269–295.
57. A. I. Hochbaum and P. Yang, *Chem.Rev.*, 2010, 110, 527-546.
58. R. Yan, D. Gargas and P. Yang, *Nature Photonics*, 2009, 3, 569–576.
59. Z. Xiong, M. Zheng, S. Liu, L. Ma and W. Shen, *Nanotechnology*, 2013, 24, 265402.
60. Y.-J. Lee, D. S. Ruby, D. W. Peters, B. B. McKenzie and J. W. P. Hsu, *Nano Lett.*, 2008, 8, 1501-1505.
61. Y. B. Tang, Z. H. Chen, H. S. Song, C. S. Lee, H. T. Cong, H. M. Cheng, W. J. Zhang, I. Bell and S. T. Lee, *Nano Lett.*, 2008, 8, 4191-4195.
62. S. L. Diedenhofen, G. Vecchi, R. E. Algra, A. Hartsuiker, O. L. Muskens, G. Immink, E. P. A. M. Bakkers, W. L. Vos and J. G. m. Rivas, *Adv.Mater.*, 2009, 21, 973–978.
63. O. L. Muskens, J. G. Rivas, R. E. Algra, E. P. A. M. Bakkers and A. Lagendijk, *Nano Lett.*, 2008, 8, 2638-2642.
64. L. Hu and G. Chen, *Nano Lett.*, 2007, 7, 3249–3252.
65. E. Garnett and P. Yang, *Nano Lett.*, 2010, 10, 1082–1087.
66. K. Peng, Y. Xu, Y. Wu, Y. Yan, S.-T. Lee and J. Zhu, *Small*, 2005, 1, 1062-1067.
67. K. Zhu, N. R. Neale, A. Miedaner and A. J. Frank, *Nano Lett.*, 2007, 7, 69-74.
68. H. W. Jeong and H. Park, *Catal.Today*, 2014, 230, 15-19.
69. J.-Y. Jung, Z. Guo, S.-W. Jee, H.-D. Um, K.-T. Park and J.-H. Lee, *Optics Express*, 2010, 18, A286–A292.
70. Z. Fan, R. Kapadia, P. W. Leu, X. Zhang, Y.-L. Chueh, K. Takei, K. Yu, A. Jamshidi, A. A. Rathore, D. J. Ruebusch, M. Wu and A. Javey, *Nano Lett.*, 2010, 10, 3823–3827.
71. X. Feng, K. Shankar, O. K. Varghese, M. Paulose, T. J. Latempa and C. A. Grimes, *Nano Lett.*, 2008, 8, 3781–3786.
72. M. Law, L. E. Greene, J. C. Johnson, R. Saykally and P. Yang, *Nature Mater.*, 2005, 4, 455-459.
73. E. Enache-Pommer, J. E. Boercker and E. S. Aydil, *Appl.Phys.Lett*, 2007, 91, 123116.
74. S. Gubbala, V. Chakrapani, V. Kumar and M. K. Sunkara, *Adv.Funct.Mater.*, 2008, 18, 2411–2418.
75. M. Law, L. E. Greene, A. Radenovic, T. Kuykendall, J. Liphardt and P. Yang, *J.Phys.Chem.B*, 2006, 110, 22652–22663.
76. J. Liang, Y. Cao, H. Lin, Z. Zhang, C. Huang and a. X. Wang, *Inorg.Chem*, 2013, 52, 6916−6922.
77. M. Yang, Y. Ji, W. Liu, Y. Wang and X. Liu, *RSC Adv.*, 2014, 4, 15048-15054.
78. Y. Qiu, S.-F. Leung, Q. Zhang, B. Hua, Q. Lin, Z. Wei, K.-H. Tsui, Y. Zhang, S. Yang and Z. Fan, *Nano Lett.*, 2014, 14, 2123-2129.
79. D. W. Hwang, H. G. Kim, J. Kim, K. Y. Cha, Y. G. Kim and J. S. Lee, *J.Catal.*, 2000, 193, 40-48.
80. S. Ikeda, M. Hara, J. N. Kondo and K. Domen, *J.Mater.Res.*, 1998, 13, 852-855.
81. H. Zhou, X. Li, T. Fan, F. E. Osterloh, J. Ding, E. M. Sabio, D. Zhang and Q. Guo, *Adv.Mater.*, 2010, 22, 951-956.

82. Z. Liu, D. D. Sun, P. Guo and J. O. Leckie, *Nano Lett.*, 2007, 7, 1081–1085.
83. G. Yang, W. Yan, Q. Zhang, S. Shen and S. Ding, *Nanoscale*, 2013, 5, 12432–12439.
84. N. Bubler, K. Meier and J.-F. Reber, *J.Phys.Chem.*, 1984, 88, 3261-3268.
85. S. K. Choi, S. Kim, J. Ryu, S. K. Lim and H. Park, *Photochem.Photobiol.Sci*, 2012, 11, 1437-1444.
86. I. E. Castelli, J.M.G.-Lastra, F. Huser, K. S. Thygesen and K. W. Jacobsen, *New J. Phys.*, 2013, 15, 105026.
87. Y. Xu and M. A. A. Schoonen, *Am. Mineral.*, 2000, 85, 543-556.
88. J. Zhang, J. Yu, Y. Zhang, Q. Li and J. R. Gong, *Nano Lett.*, 2011, 11, 4774-4779.
89. I. Gorczyca, T. Suski, N. E. Christensen and A. Svane, *Appl.Phys.Lett*, 2010, 96, 101907.
90. S. Burnside, J.-E. Moser, K. Brooks and M. Grätzel, *J. Phys. Chem. B*, 1999, 103, 9328-9332.
91. S.-C. Chiu and Y.-Y. Li, *J. Cryst. Growth*, 2009, 311, 1036-1041.
92. T. A. Kandiel, A. Feldhoff, L. Robben, R. Dillert and D. W. Bahnemann, *Chem.Mater.*, 2010, 22, 2050-2060.
93. J. Jitputti, Y. Suzuki and S. Yoshikawa, *Catal.Commun.*, 2008, 9, 1265-1271.
94. L. Kavan, M. Gratzel, S. E. Gilbert, C. Klemenz and H. J. Scheel, *J. Am. Chem. Soc.*, 1996, 118, 6716-6723.
95. B. Ohtani, Y. Ogawa and S.-i. Nishimoto, *J.Phys.Chem.B*, 1997, 101, 3746-3752.
96. H. Kominami, Y. Ishii, M. Kohno, S. Konishi, Y. Kera and B. Ohtani, *Catal. Lett*, 2003, 91, 41-47.
97. L. Yan, J. Zhang, X. Zhou, X. Wu, J. Lan, Y. Wang, G. Liu, J. Yu and L. Zhi, *Int.J.Hydrogen Eng.*, 2013, 38, 3554-3561.
98. S. E. Braslavsky, A. M. Braun, A. E. Cassano, A. V. Emeline, M. I. Litter, L. Palmisano, V. N. Parmon and N. Serpone, *Pure Appl.Chem.,*, 2011, 83, 931-1014.
99. X. Chen and S. S. Mao, *Chem.Rev.*, 2007, 107, 2891–2959.
100. Y. Lee, T. Watanabe, T. Takata, M. Hara, M. Yoshimura and K. Domen, *Bull. Chem. Soc. Japn*, 2007, 80, 423 - 428.
101. Z. Zhang, C.-C. Wang, R. Zakaria and J. Y. Ying, *J.Phys.Chem.B*, 1998, 102, 10871–10878.
102. W. Sun, S. Zhang, Z. Liu, C. Wang and Z. Mao, *Int.J.Hydrogen Eng.*, 2008, 33, 1112-1117.
103. P. V. Kamat, *J.Phys.Chem.C*, 2007, 111, 2834-2860.
104. N. Bao, L. Shen, T. Takata, D. Lu and K. Domen, *Chem.Lett.*, 2006, 35, 318-319.
105. H. Liu, J. Yang, J. Liang, Y. Huang and C. Tang, *J.Am.Ceram.Soc*, 2008, 91, 1287–1291.
106. J. S. Jang, S. H. Choi, D. H. Kim, J. W. Jang, K. S. Lee and J. S. Lee, *J.Phys.Chem.C*, 2009, 113, 8990–8996.
107. J. Jitputti, S. Pavasupree, Y. Suzuki and S. Yoshikawa, *Jpn.J.Appl.Phys.*, 2008, 47, 751-756.
108. Z. Jiang, F. Yang, N. Luo, B. T. T. Chu, D. Sun, H. Shi, T. Xiao and P. P. Edwards, *Chem.Commun*, 2008, 47, 6372-6374
109. S. Palmas, A. M. Polcaro, J. R. Ruiz, A. D. Pozzo, M. Mascia and A. Vacca, *Int.J.Hydrogen Eng.*, 2010, 35, 6561-6570.
110. J. Yu, H. Yu, B. Cheng and C. Trapalis, *J.Molecular Catal. A*, 2006, 249, 135-142.
111. H. Jia, W.-J. Xiao, L. Zhang, Z. Zheng, H. Zhang and F. Deng, *J.Phys.Chem.C*, 2008, 112, 11379–11384.
112. Y. Wang, L. Zhang, K. Deng, X. Chen and Z. Zou, *J.Phys.Chem.C*, 2007, 111, 2709–2714.
113. Y. Li, Y. Hu, S. Peng, G. Lu and S. Li, *J.Phys.Chem.C*, 2009, 113, 9352–9358.
114. Y. Li, T. Sasaki, Y. Shimizu and N. Koshizaki, *J.Am.Chem.Soc.*, 2008, 130, 14755–14762.
115. F. A. Frame, E. C. Carroll, D. S. Larsen, M. Sarahan, N. D. Browning and F. E. Osterloh, *Chem.Commun*, 2008, 19, 2206–2208.
116. D. Chen and J. Ye, *Chem.Mater.*, 2009, 21, 2327–2333.
117. S. Chuangchote, J. Jitputti, T. Sagawa and S. Yoshikawa, *ACS Appl.Mater.Interfaces*, 2009, 1, 1140–1143.
118. Z. Zhang, Z. Wang, S.-W. Cao and C. Xue, *J.Phys.Chem.C*, 2013, 117, 25939−25947.
119. S. S. Lee, H. Bai, Z. Liu and D. D. Sun, *Int.J.Hydrogen Eng.*, 2012, 37, 10575-10584.
120. L. Macaraig, S. Chuangchote and T. Sagawa, *J.Mater.Res.*, 2014, 29, 123-130.
121. H. Bai, Z. Liu and D. D. Sun, *J.Am.Ceram.Soc*, 2013, 96, 942-949.
122. X. Yang, A. Wolcott, G. Wang, A. Sobo, R. C. Fitzmorris, F. Qian, J. Z. Zhang and Y. Li, *Nano Lett.*, 2009, 9, 2331-2336.
123. J. Jitputti, S. Pavasupree, Y. Suzuki and S. Yoshikawa, *J.Solid State Chem.*, 2007, 180, 1743-1749.
124. A. Patsoura, D. I. Kondarides and X. E. Verykios, *Catal.Today*, 2007, 124, 94-102.
125. A. Galin´ska and J. Walendziewski, *Energy & Fuels*, 2005, 19, 1143-1147.
126. P. Tongying, F. Vietmeyer, D. Aleksiuk, G. J. Ferraudi, G. Krylova and M. Kuno, *Nanoscale*, 2014, 6, 4117-4124.
127. M.-C. Wu, J. Hiltunen, A. Sapi, A. Avila, W. Larsson, H.-C. Liao, M. Huuhtanen, G. Toth, A. Shchukarev, N. Laufer, A. Kukovecz, Z. Konya, J.-P. Mikkola, R. Keiski, W.-F. Su, Y.-F. Chen, H. Jantunen, P. M. Ajayan, R. Vajtai and K. Kordas, *ACS Nano*, 2011, 5, 5025–5030.
128. G. K. Mor, H. E. Prakasam, O. K. Varghese, K. Shankar and C. A. Grimes, *Nano Lett.*, 2007, 7, 2356-2364.
129. G. K. Mor, K. Shankar, M. Paulose, O. K. Varghese and C. A. Grimes, *Nano Lett.*, 2005, 5, 191-195.
130. O. K. Varghese, M. Paulose, K. Shankar, G. K. Mor and C. A. Grimes, *J.Nanosci.Nanotechnol.*, 2005, 5, 1158–1165.
131. K. Shankar, G. K. Mor, H. E. Prakasam, S. Yoriya, M. Paulose, O. K. Varghese and C. A. Grimes, *Nanotechnology*, 2007, 18, 065707.
132. G. K. Mor, O. K. Varghese, R. H. T. Wilke, S. Sharma, K. Shankar, T. J. Latempa, K.-S. Choi and C. A. Grimes, *Nano Lett.*, 2008, 8, 1906-1911.
133. D. Eder, M. Motta and A. H. Windle, *Nanotechnology*, 2009, 20, 055602.
134. J. H. Park, S. Kim and A. J. Bard, *Nano Lett.*, 2006, 6, 24-28.
135. W. H. Lubberhuizen, D. Vanmaekelbergh and E. V. Faassen, *J.Porous Mater.*, 2000, 7, 147-152.
136. A. F. Feil, P. Migowski, F. R. Scheffer, M. D. Pierozan, R. R. Corsetti, M. Rodrigues, R. P. Pezzi, G. Machado, L. Amaral,

S. R. Teixeira, D. E. Weibel and J. Dupont, *J.Braz.Chem.Soc*, 2010, 21, 1359-1365.
137.Y.-C. Pu, G. Wang, K.-D. Chang, Y. Ling, Y.-K. Lin, B. C. Fitzmorris, C.-M. Liu, X. Lu, Y. Tong, J. Z. Zhang, Y.-J. Hsu and Y. Li, *Nano Lett.*, 2013, 13, 3817−3823.
138.A. Wood, M. Giersig and P. Mulvaney, *J. Phys. Chem. B*, 2001, 105, 8810–8815.
139.T.-C. Pan, S.-H. Wang, Y.-S. Lai, J.-M. Jehng and S.-J. Huang, *Appl.Surface Sci.*, 2014, 296, 189-194.
140.M. Ye, J. Gong, Y. Lai, C. Lin and Z. Lin, *J. Am. Chem. Soc.*, 2012, 134, 15720−15723.
141.F.-C. Wang, C.-H. Liu, C.-W. Liu, J.-H. Chao and C.-H. Lin, *J.Phys.Chem.C*, 2009, 113, 13832-13840.
142.R. P. Antony, T. Mathews, C. Ramesh, N. Murugesan, A. Dasgupta, S. Dhara, S. Dash and A. K. Tyagi, *Int. J. Hydrogen Energ.*, 2012, 37, 8268-8276.
143.X. Wang, G. Liu, Z.-G. Chen, F. Li, G. Q. M. Lu and H.-M. Cheng, *Electrochem.Commun.*, 2009, 11, 1174-1178.
144.M. P. Languer, F. R. Scheffer, A. F. Feil, D. L. Baptista, P. Migowski, G. J. Machado, D. P. d. Moraes, J. Dupont, S. R. Teixeira and D. E. Weibel, *Int.J.Hydrogen Eng.*, 2013, 38, 14440-14450.
145.Y. Li, H. Yu, C. Zhang, W. Song, G. Li, Z. Shao and B. Yi, *Elecrochim.Acta*, 2013, 107, 313–319.
146.J. Gong, Y. Lai and C. Lin, *Elecrochim.Acta*, 2010, 55, 4776-4782.
147.J. Gong, W. Pu, C. Yang and J. Zhang, *Catal.Commun.*, 2013, 36, 89-93.
148.R. V. Gonçalves, P. Migowski, H. Wender, D. Eberhardt, D. E. Weibel, F. v. C. Sonaglio, M. J. M. Zapata, J. Dupont, A. F. Feil and S. R. Teixeira, *J.Phys.Chem.C*, 2012, 116, 14022−14030.
149.M. Cargnello, M. Grzelczak, B. R.-G.´lez, Z. Syrgiannis, K. Bakhmutsky, V. L. Parola, L. M. L.-M.´, R. J. Gorte, M. Prato and P. Fornasiero, *J. Am. Chem. Soc.*, 2012, 134, 11760-11766.
150.*Chem. Rev.*, 2014, 114, 9281-10216.
151.Y. Lee, T. Watanabe, T. Takata, M. Hara, M. Yoshimura and K. Domen, *Bull. Chem. Soc. Japn*, 2007, 80, 423- 428.
152.H. Bai, Z. Liu and D. D. Sun, *J.Mater.Chem*, 2012, 22, 18801-18807.
153.B. M. Kayes, H. A. Atwater and N. S. Lewis, *J.Appl.Phys.*, 2005, 97, 114302.
154.D. Chen and J. Ye, *Chem.Mater.*, 2007, 19, 4585-4591.
155.Y. Sun, W. D. Chemelewski, S. P. Berglund, C. Li, H. He, G. Shi and C. B. Mullins, *ACS Appl.Mater.Interfaces*, 2014, 6, 5494−5499.
156.B. Sun, T. Shi, Z. Peng, W. Sheng, T. Jiang and G. Liao, *Nanoscale Res. Lett.*, 2013, 8, 462.
157.K. Lin, B. Ma, W. Su and W. Liu, *Appl.Surface Sci.*, 2013, 286, 61-65.
158.J. Liang, J. Xu, Q. Gu, Y. Zhou, C. Huang, H. Lin and X. Wang, *J.Mater.Chem.A*, 2013, 1, 7798–7805.
159.X. Yang, J. Xu, T. Wong, Q. Yang and C.-S. Lee, *Phys.Chem.Chem.Phys.*, 2013, 15, 12688--12693.
160.D. Li and Y. Xia, *Adv.Mater.*, 2004, 16, 1151-1170.
161.A. Greiner and J. H. Wendorff, *Angew. Chem. Int. Ed.* , 2007, 46, 5670-5703.
162.D. H. Reneker and A. L. Yarin, *Polymer*, 2008, 49, 2387e2425.
163.X. Lu and C. W. a. Y. Wei, *Small*, 2009, 5, 2349-2370.
164.S. J. Limmer, *Adv.Mater.*, 2003, 15, 427-431.
165.Z. Miao, D. Xu, J. Ouyang, G. Guo, X. Zhao and Y. Tang, *Nano Lett.*, 2002, 2, 717-720.
166.M. Adachi, Y. Murata, J. Takao, J. Jiu, M. Sakamoto and F. Wang, *J.Am.Chem.Soc.*, 2004, 126, 14943–14949.
167.Y.-w. Jun, M. F. Casula, J.-H. Sim, S. Y. Kim, J. Cheon and A. P. Alivisatos, *J.Am.Chem.Soc.*, 2003, 125, 15981–15985.
168.J.-M. Wu, H. C. Shih and W.-T. Wu, *Nanotechnology*, 2006, 17, 105-109.
169.Z. R. Tian, J. A. Voigt, J. Liu, B. Mckenzie and H. Xu, *J.Am.Chem.Soc.*, 2003, 125, 12384–12385.
170.V. S. P. Kumar, V. J. Babu, G. K. Raghuraman, R. Dhamodharan and T. S. Natarajan, *J. Appl. Phys.*, 2007, 101, 114317.
171.V. J. Babu, S. Vempati and S. Ramakrishna, *RSC Adv.*, 2014, 4, 27979-27987.
172.F. Kayaci, S. Vempati, I. Donmez, N. Biyikli and T. Uyar, *Nanoscale*, 2014, 6, 10224-10234.
173.F. Kayaci, S. Vempati, C.O.-Akgun, N. Biyikli and T. Uyar, *Appl. Catal. B.*, 2014, 156-157, 173-183.
174.V. J. Babu, R. S. R. Bhavatharini and S. Ramakrishna, *RSC Adv.*, 2014, 4, 29957-29963.
175.M. M. Khin, S. Nair, J. B. Veluru, M. Rajendiran and S. Ramakrishna, *Energ. Environ. Sci.*, 2012.
176.V. J. Babu, S. Vempati, S. Sundarrajan, M. Sireesha and S. Ramakrishna, *Solar Energy*, 2014, 106, 1-22.
177.Y.-Z. Long, M. Yu, B. Sun, C.-Z. Gu and Z. Fan, *Chem.Soc.Rev.*, 2012, 41, 4560–4580.
178.C. J. Luo, S. D. Stoyanov, E. Stride, E. Pelan and M. Edirisinghe, *Chem.Soc.Rev*, 2012, 41, 4708-4735
179.A. A. Madhavan, S. Kalluri, D. K. Chacko, T. A. Arun, S. Nagarajan, K. R. V. Subramanian, A. S. Nair, S. V. Nair and A. Balakrishnan, *RSC Adv.*, 2012, 2, 13032–13037.
180.G. Dong, X. Xiao, L. Zhang, Z. Ma, X. Bao, M. Peng, Q. Zhang and J. Qiu, *J.Mater.Chem.*, 2011, 21, 2194-2203.
181.A. Babel, D. Li, Y. Xia and S. A. Jenekhe, *Macromolecules*, 2005, 38, 4705–4711.
182.M. Tanveer, A. Habib and M. B. Khan, *J.Expt. Nanoscience*, 2014, xx, xxx-xxx.
183.P. Ahmadpoor, A. S. Nateri and V. Motaghitalab, *J.Appl.Polym.Sci*, 2013, 130, 78-85.
184.L. Gao and C. Li, *J.Luminescence*, 2010, 130, 236-239.
185.M. A. Kanjwal, N. A. M. Barakat, F. A. Sheikh, D. K. Park and H. Y. Kim, *J.Mater.Sci.*, 2010, 45, 3833–3840.
186.J. B. Veluru, K. K. Satheesh, D. C. Trivedi, M. V. Ramakrishna and T. N. Srinivasan, *Journal of Engineered Fibers and Fabrics*, 2007, 2, 25.
187.S. Vempati, J. B. Veluru, R. G. Karunakaran, D. Raghavachari and T. S. Natarajan, *J. Appl. Phys.*, 2011, 110, 113718.
188.M. M. Munir, F. Iskandar, K. M. Yun, K. Okuyama and M. Abdullah, *Nanotechnology*, 2008, 19, 145603.
189.J.-Y. Chen, C.-C. Kuo, C.-S. Lai, W.-C. Chen and H.-L. Chen, *Macromolecules*, 2011, 44, 2883–2892.
190.C. Drew, X. Liu, D. Ziegler, X. Wang, F. F. Bruno, J. Whitten, L. A. Samuelson and J. Kumar, *Nano Lett.*, 2003, 3, 143-147.

191.B. Ding, M. Wang, J. Yu and G. Sun, *Sensors*, 2009, 9, 1609-1624.

192.H. Wu, L. Hu, M. W. Rowell, D. Kong, J. J. Cha, J. R. McDonough, J. Zhu, Y. Yang, M. D. McGehee and Y. Cui, *Nano Lett.*, 2010, 10, 4242–4248.

193.Y. Shmueli, G. E. Shter, O. Assad, H. Haick, P. Sonntag, P. Ricoux and G. S. Grader, *J.Mater.Res.*, 2012, 27, 1672-1679.

194.A. Kumar, R. Jose, K. Fujihara, J. Wang and S. Ramakrishna, *Chem.Mater.*, 2007, 19.

195.D. Hou, X. Hu, Y. Wen, B. Shan, P. Hu, X. Xiong, Y. Qiao and Y. Huang, *Phys.Chem.Chem.Phys.*, 2013, 15, 20698-20705.

196.V. J. Babu, S. Vempati, G. J. Subha, V. Kumari, T. S. Natarajan, A. S. Nair and S. Ramakrishna, *Journal of Engineered Fibers and Fabrics*, 2011, 6, 57-59.

197.V. J. Babu, V. S. P. Kumar, B. Sundaray, V. R. K. Murthy and T. S. Natarjan, *Mater.Sci.Eng.B*, 2007, 142, 46-50.

198.H. Bai, J. Juay, Z. Liu, X. Song, S. S. Lee and D. D. Sun, *Appl.Catal.B:Environ*, 2012, 125, 367-374.

199.T. Sun, J. Qiu and C. Liang, *J.Phys.Chem.C*, 2008, 112, 715-721.

200.W.-W. Wang, Y.-J. Zhu and L.-X. Yang, *Adv.Funct.Mater.*, 2007, 17, 59–64.

201.S. Xiong, B. Xi, C. Wang, G. Xi and X. L. a. Y. Qian, *Chem.Eur.J.*, 2007, 13, 7926–7932.

202.T.-G. Xu, C. Zhang, X. Shao, K. Wu and Y.-F. Zhu, *Adv.Funct.Mater.*, 2006, 16, 1599–1607.

203.Y. Matsumoto, S. Ida and T. Inoue, *J.Phys.Chem.C*, 2008, 112, 11614-11616.

204.E. C. Carroll, O. C. Compton, D. Madsen, F. E. Osterloh and D. S. Larsen, *J.Phys.Chem.C*, 2008, 112, 2394–2403.

205.C. Ye, Y. Bando, G. Shen and D. Golberg, *J.Phys.Chem.B*, 2006, 110, 15146–15151.

206.C. Zhang and Y. Zhu, *Chem.Mater.*, 2005, 17, 3537-3545.

207.V. J. Babu, S. R. S. Bhavatharini and S. Ramakrishna, *RSC Adv.*, 2014, 4, 19251-19256.

208.S. H. Kim, S. Park, C. W. Lee, B. S. Han, S. W. Seo, J. S. Kim, I. S. Cho and K. S. Hong, *Int.J.Hydrogen Eng.*, 2012, 37, 16895–16902.

209.K. Parida, M. Satpathy and L. Mohapatra, *J.Mater.Chem*, 2012, 22, 7350-7357.

210.L. Zhao, J. Ran, Z. Shu, G. Dai, P. Zhai and S. Wang, *Int.J.Photoenergy*, 2012, 2012, Article ID 472958.

211.Z. Li, J. Shen, J.-Q. Wang, D. Wang, Y. Huang and J. Zou, *Cryst.Eng.Comm*, 2012, 14, 1874-1880.

212.O. C. Compton and F. E. Osterloh, *J.Phys.Chem.C*, 2009, 113, 479-485.

213.M. Harada, T. Sasaki, Y. Ebina and M. Watanabe, *J.Photochem.Photobiol.A.*, 2002, 148, 273-276.

214.L. Zhang, D. Chen and X. Jiao, *J.Phys.Chem.B*, 2006, 110, 2668–2673.

215.X. Zhang, Z. Ai, F. Jia and L. Zhang, *J.Phys.Chem.C*, 2008, 112, 747-753.

216.M. C. Sarahan, E. C. Carroll, M. Allen, D. S. Larsen, N. D. Browning and F. E. Osterloh, *J.Solid State Chem.*, 2008, 181, 1678-1683.

217.J. Yu, L. Qi and M. Jaroniec, *J.Phys.Chem.C*, 2010, 114, 13118-13125.

218.G. Xiang, T. Li, J. Zhuang and X. Wang, *Chem.Commun*, 2010, 46, 6801-6803.

219.J. Jitputti, T. Rattanavoravipa, S. Chuangchote, S. Pavasupree, Y. Suzuki and S. Yoshikawa, *Catal.Commun.*, 2009, 10, 378-382.

220.O. C. Compton, E. C. Carroll, J. Y. Kim, D. S. Larsen and F. E. Osterloh, *J.Phys.Chem.C*, 2007, 111, 14589–14592.

221.O. C. Compton, C. H. Mullet, S. Chiang and F. E. Osterloh, *J.Phys.Chem.C*, 2008, 112, 6202-6208.

222.X. Chen, S. Shen, L. Guo and S. S. Mao, *Chem. Rev.*, 2010, 110, 6503-6570.

223.M. Machida, X. W. Ma, H. Taniguchi, J.-i. Yabunaka and T. Kijima, *J.Molecular Catal. A*, 2000, 155, 131-142.

224.T. Sasaki, *J.Ceram.Soc.Jpn*, 2007, 115, 9-16.

225.T. Yamase, *Chem.Rev.*, 1998, 98, 307-326.

226.E. M. Sabio, R. L. Chamousis, N. D. Browning and F. E. Osterloh, *J.Phys.Chem.C*, 2012, 116, 3161-3170.

227.Y. Zhang, T. Xia, M. Shang, P. Wallenmeyer, D. Katelyn, A. Peterson, J. Murowchick, L. Dong and X. Chen, *RSC Adv.*, 2014, 4, 16146–16152.

228.S. S. Lee, H. Bai, Z. Liu and D. D. Sun, *Water Research*, 2013, 47, 4059-4073.

229.J. S. Jang, U. A. Joshi and J. S. Lee, *J. Phys. Chem. C*, 2007, 111, 13280-13287.

230.N. Buhler, K. Meier and J.-F. Reber, *J. Phys. Chem.*, 1984, 88, 3261-3268.

231.J. Zhang, Y. Wang, J. Jin, J. Zhang, Z. Lin, F. Huang and J. Yu, *ACS Appl.Mater.Interfaces*, 2013, 5, 10317−10324.

232.Q. Li and G. Lu, *J.Power Sources*, 2008, 185, 577-583.

233.M. G. Kibria, S. Zhao, F. A. Chowdhury, Q. Wang, H. P. T. Nguyen, M. L. Trudeau, H. Guo and Z. Mi, *Nat.Commun.*, 2014, 5, 3825.

234.C. Li, J. Yuan, B. Han, L. Jiang and W. Shangguan, *Int. J. Hydrogen Energ.*, 2010, 35, 7073-7079.

235.C. Liu, J. Tang, H. M. Chen, B. Liu and P. Yang, *Nano Lett.*, 2013, 13, 2989−2992.

236.M. G. Kibria, H. P. T. Nguyen, K. Cui, S. Zhao, D. Liu, H. Guo, M. L. Trudeau, S. Paradis, A.-R. Hakima and Z. Mi, *ACS Nano*, 2013, 7, 7886–7893

237.K. Maeda, N. Sakamoto, T. Ikeda, H. Ohtsuka, A. Xiong, D. Lu, M. Kanehara, T. Teranishi and K. Domen, *Chem. Eur. J*, 2010, 16, 7750-7759.

238.B. AlOtaibi, H. P. T. Nguyen, S. Zhao, M. G. Kibria, S. Fan and Z. Mi, *Nano Lett.*, 2013, 13, 4356−4361.

239.S. Vempati, S. Chirakkara, J. Mitra, P. Dawson, K. K. Nanda and S. B. Krupanidhi, *Appl. Phys. Lett.*, 2012, 100, 162104.

240.S. Vempati, J. Mitra and P. Dawson, *Nanoscale Res. Lett.*, 2012, 7, 470.

241.S. Vempati, A. Shetty, P. Dawson, K. Nanda and S. B. Krupanidhi, *J. Cryst. Growth*, 2012, 343, 7-12.

242.S. Vempati, A. Shetty, P. Dawson, K. K. Nanda and S. B. Krupanidhi, *Thin Solid Films*, 2012, 524, 137-143.

243.Q. Kang, J. Cao, Y. Zhang, L. Liu, H. Xu and J. Ye, *J. Mater. Chem. A*, 2013, 1, 5766-5774.

244.Y. Liu, H. Zhou, B. Zhou, J. Li, H. Chen, J. Wang, J. Bai, W. Shangguan and W. Cai, *Int. J. Hydrogen Energ.*, 2011, 36, 167-174.

245.Q. Li and G. Lu, *J. Mol. Catal A-Chem*, 2007, 266, 75–79.

246.Q. Li, L. Chen and G. Lu, *J.Phys.Chem.C*, 2007, 111, 11494-11499.

247.G. Khan, S. K. Choi, S. Kim, S. K. Lim, J. S. Jang and H. Park, *Appl. Catal. B Environ.*, 2013, 142-143, 647-653.
248.S. K. Parayil, J. Baltrusaitis, C.-M. Wu and R. T. Koodali, *Int. J. Hydrogen Energ.*, 2013, 38, 2656-2669.
249.P. Khemthong, P. Photai and N. Grisdanurak, *Int. J. Hydrogen Energ.*, 2013, 38, 15992-16001.
250.J. Ran, J. Yu and M. Jaroniec, *Green Chem*, 2011, 13, 2708–2713.
251.N. S. Chaudhari, S. S. Warule, S. Muduli, B. B. Kale, S. Jouen, B. Lefez, B. Hannoyer and S. B. Ogale, *Dalton Trans*, 2011, 40, 8003–8011.
252.H. Lv, L. Ma, P. Zeng, D. Ke and T. Peng, *J.Mater.Chem*, 2010, 20, 3665–3672.
253.S. Mubeen, J. Lee, N. Singh, S. Kra¨mer, G. D. Stucky and M. Moskovits, *Nat.Nanotech.*, 2013, 8, 247-251.
254.S. S. Lee, H. Bai, Z. Liu and D. D. Sun, *Appl.Catal.B*, 2013, 140, 68-81.
255.Z. Zhang, A. Li, S.-W. Cao, M. Bosman, S. Li and C. Xue, *Nanoscale*, 2014, 6, 5217–5222.
256.A. Yousef, N. A. M. Barakat, K. A. Khalil, A. R. Unnithan, G. Panthi, B. Pant and H. Y. Kim, *Colloids and Surfaces A*, 2012, 410, 59-65.
257.N. Sobti, A. Bensouici, F. Coloma, C. Untiedt and S. Achour, *J.Nanopart.Res*, 2014, 16, 2577.
258.A. R. Unnithan, N. A. M. Barakat, R. Nirmala, S. S. Al-Deyab and H. Y. Kim, *Ceram. Int.*, 2012, 38, 5175-5180.
259.Q. Li, X. Sun, K. Lozano and Y. Mao, *J.Phys.Chem.C*, 2014, 118, 13467−13475.
260.N. Bao, L. Shen, T. Takata and K. Domen, *Chem.Mater.*, 2008, 20, 110-117.
261.Z. Lei, W. You, M. Liu, G. Zhou, T. Takata, M. Hara, K. Domen and C. Li, *Chem. Comm.*, 2003, 2142-2143.
262.S. Siol, H. Strater, R. Bruggemann, J. Brotz, G. H. Bauer, A. Klein and W. Jaegermann, *J. Phys. D. Appl. Phys.*, 2013, 46, 495112.
263.X. Li, H. Shen, S. Li, J. Z. Niu, H. Wang and L. S. Li, *J. Mater. Chem.*, 2010, 20, 923-928.
264.S. Panigrahi and D. Basak, *RSC Adv.*, 2012, 2, 11963-11968.
265.Z. Khan, M. Khannam, N. Vinothkumar, M. De and M. Qureshi, *J.Mater.Chem.*, 2012, 22, 12090–12095.
266.Q. Li, B. Guo, J. Yu, J. Ran, B. Zhang, H. Yan and J. R. Gong, *J. Am. Chem. Soc.*, 2011, 133, 10878–10884.
267.Y. Li, Y.-L. Li, C. M. Araujo, W. Luo and R. Ahuja, *Catal.Sci.Technol*, 2013, 3, 2214--2220.
268.Z. Xu, Y. Li, S. Peng, G. Lu and S. Li, *RSC Adv.*, 2012, 2, 3458-3466.
269.X. Bai and J. Li, *Mater.Res.Bull*, 2012, 46, 1028-1034.
270.F. A. Frame and F. E. Osterloh, *J.Phys.Chem.C*, 2010, 114, 10628–10633.
271.X. Wang, K. Maeda, A. Thomas, K. Takanabe, G. Xin, J. M. Carlsson, K. Domen and M. Antonietti, *Nat. Mater.*, 2008, 8, 76-80.
272.X. Wang, K. Maeda, X. Chen, K. Takanabe, K. Domen, Y. Hou, X. Fu and M. Antonietti, *J. Am. Chem. Soc.*, 2009, 131, 1680–1681.
273.J. Liu, J. Huang, H. Zhou and M. Antonietti, *ACS Appl.Mater.Interfaces*, 2014, 6, 8434-8440.
274.J. Huang, M. Antonietti and J. Liu, *J.Mater.Chem.A*, 2014, 2, 7686–7693.
275.A. Yousef, N. A. M. Barakat and H. Y. Kim, *Appl. Catal. A Gen.*, 2013, 467, 98-106.
276.*http://energy.gov/eere/fuelcells/market-analysis-reports*.
277.K. Maeda, H. Hashiguchi, H. Masuda, R. Abe and K. Domen, *J.Phys.Chem.C*, 2008, 112, 3447-3452.
278.K. Nishijima, T. Kamai, N. Murakami, T. Tsubota and T. Ohno, *Int.J.Photoenergy*, 2008, 2008, Article ID 173943.
279.J. Tang, J. R. Durrant and D. R. Klug, *J. Am. Chem. Soc.*, 2008, 130, 13885-13891.